Surface engineering of silica nanoparticles with a gadolinium-PCTA complex for efficient T_1-weighted MRI contrast agents.

Paul Mathieu[1, 2], Marie Chalet[3,4], Marie Myriam Clain[3,4], Lauryanne Teulon[1, 2], Eric Benoist[3,4], Nadine Leygue[3,4], Claude Picard[3,4], Sébastien Boutry[5,6], Sophie Laurent[5,6], Dimitri Stanicki[5], Céline Hénoumont[5], Fernando Novio[7], Julia Lorenzo[8], David Montpeyó[8], Diana Ciuculescu-Pradines,[1,2] Catherine Amiens[1, 2].

[1] CNRS, LCC (Laboratoire de Chimie de Coordination), 205 route de Narbonne, BP 44099, F-31077 Toulouse Cedex 4, France.
[2] Université de Toulouse, UPS, INPT, F-31077 Toulouse Cedex 4, France.
[3] CNRS, Laboratoire de Synthèse et Physico-Chimie de Molécules d'Intérêt Biologique (SPCMIB), UMR- 5068, 118 Route de Narbonne, 31062 Toulouse cedex 9, France.
[4] Université de Toulouse, UPS, Laboratoire de Synthèse et Physico-Chimie de Molécules d'Intérêt Biologique, SPCMIB, Toulouse, France.
[5] Department of General, Organic and Biomedical Chemistry, NMR and Molecular Imaging Laboratory, University of Mons, 19 avenue Maistriau, B- 7000 Mons, Belgium.
[6] Center for Microscopy and Molecular Imaging (CMMI), Université de Mons (UMONS), B-6041 Charleroi, Belgium
[7] Departament de Química, Universitat Autònoma de Barcelona (UAB), Campus UAB, 08193 Cerdanyola del Vallès, Barcelona, Spain
[8] Institut de Biotecnologia i Biomedicina, Departament de Bioquímica i de Biologia Molecular, Universitat Autònoma de Barcelona, 08193 Bellaterra, Spain.

Abstract

New pyridine containing triAza; 3,6,9,15-tetraazabicyclo[9.3.1]pentadeca-1(15),11,13-triene-3,6,9-triacetic acid (PCTA) ligands presenting pendant carboxylic acid or alcohol functions have been synthesized and used to form diaqua Gd(III) complexes, which have been immobilized onto dense silica nanoparticles. Cytotoxicity studies of these complexes (free or immobilized on the nanoparticles) on normal 1BR3G cells and cancerous HCT 116 cells indicated a dependence on the pendant chemical group for the free complexes. However, this effect disappeared once the complexes were immobilized on the surface of the nanoparticles, leading to non-toxic nanomaterials. The interest of these complexes (free or immobilized on dense silica nanoparticles) as contrast agents in magnetic resonance imaging (MRI) has been evaluated in comparison with DOTAREM® by recording their nuclear magnetic resonance dispersion (NMRD) profiles, measuring their transversal and longitudinal relaxivities as well as recording images on phantoms at 37°C. This study has evidenced the high potential of these complexes: first it suggested the possibility to reduce the dose to be injected by a factor of 10, second it evidenced their high efficiency in high field T_1-weighted MRI (9.4T), the key towards images of higher resolution and shorter acquisition times.

Introduction :

Magnetic Resonance Imaging (MRI) is a versatile imaging technique with impressive spatial resolution but poor sensitivity.[1] Today, the use of MRI contrast agents (CAs) is required in 30 % of all MRI procedures worldwide. These contrast agents are mainly Gd(III) chelates, among which DOTAREM® and MAGNEVIST® are the most used nowadays, mostly to detect tumors at an early stage, or vascular deficiencies in the body and the brain. Reaching a good signal over noise in MRI, requires injection of a rather large dose of these Gd(III) chelates (ten to twenty mL of a 0.5 mM solution depending on body weight). Engineering of thermodynamically and kinetically stable chelates is thus required to efficiently prevent the leaching of free, highly toxic, Gd(III) ions which may cause multiple adverse effects such as nephrogenic systemic fibrosis.[1] This has motivated a large research effort for the design and synthesis of adapted ligand cages.[2,3]

A large research effort also focuses on improving the effect of the contrast agents in order to be able to reduce the dose injected to the patient.[4,5]

The working principle of the Gd-based CAs relies on the effect of the paramagnetic Gd(III) center on the longitudinal relaxation rate R_1 of the water protons. Indeed, when water molecules diffuse close to this paramagnetic center (outer sphere mechanism) or exchange with water molecules coordinated to the Gd(III) center (inner sphere mechanism), their relaxation rate R_1 is increased, which increases the signal recovered in MRI, in a proportion which varies linearly with the concentration in CA introduced.[6,7] The proportional factor is called relaxivity. It is a characteristic value of a CA which depends on the temperature and strength of the magnetic field at which the MRI images are collected, and on the number of water molecules in the first coordination sphere of the CA (among other parameters). One strategy to get more efficient CAs, i.e. CA with a higher relaxivity, is to design ligand cages allowing a larger number of water molecules (q) to coordinate to the metal center. For example, the CAs cited above, DOTAREM® and MAGNEVIST® have a relatively low relaxivity (r_1 ~3.5-3.8 $mM^{-1}.s^{-1}$ at 20MHz and 37°C) due to the sole water molecule coordinated to the Gd(III) center while bis and tri-hydrated complexes display up to twice larger values.[8,9] But these results should be taken with care as some of these complexes are less stable than the mono-aquacoordinated complexes[7,10] leading to a possible release of toxic Gd(III) ions in the body over time. In this context PCTA (Pyridine Containing TriAza; 3,6,9,15-tetraazabicyclo[9.3.1]pentadeca-1(15),11,13-triene-3,6,9-triacetic acid) cages offer a good compromise by providing Gd complexes with increased hydration number (q=2) yielding a longitudinal relaxivity value r_1 of 5.8 $mM^{-1}.s^{-1}$ (20MHz, 37°C)[11] and thermodynamic and kinetic constants close to those of the CAs currently in use.

However, molecular CAs also suffer from the fact that their relaxivity is highest at low fields (<10MHz) while the pursuit of improved spatial resolution pushes the development of MRI machines towards high operating fields.[12] At magnetic fields currently used in clinics (20-60MHz), the efficiency of molecular CAs is not optimum.[13] One of the keys to improve the relaxivity and range of accessible imaging fields consists in reducing the rotational correlation time (τ_R) of the complex to favour the propagation of the paramagnetic effect of

the Gd(III) ion through the chains of hydrogen bounded water molecules. One easy way to do so is to immobilize the CA on/in a bigger and heavier moiety such as micelles, liposomes, organic or inorganic nanoparticles (NPs).[6] It presents the added advantage of increasing the residence time of the CA in the body thus overcoming another drawback of Gd(III) chelates which is their very fast clearance.[14] Care should be taken at this stage to ensure a good access of the water molecules to the Gd(III) center. As such, surface immobilization gives the best results.[15,16]

Based on the above considerations, we investigated the grafting of stable bis-hydrated Gd(III) complexes (Figure 1) on preformed dense silica NPs as a possible way to overcome the issues raised above. Gd(III) ions were chelated by PCTA ligands for their well-known efficiency to coordinate lanthanide ions with high thermodynamic stability, kinetic inertness and *in vivo* stability while allowing two water molecules into the coordination sphere.[17–19] Also, the parent Gd-PCTA complex displays a short residence lifetime of the inner-sphere water molecules (τ_M 310K = 82 ns), a favourable factor for providing high relaxivity once the chelate will be immobilized by covalent binding to NPs.[11] In this paper, two grafting strategies, depicted in Figure 2, are compared (amidic coupling versus condensation) and the best samples have been evaluated in MRI in comparison to the free complexes and DOTAREM®. A first evaluation of their cytotoxicity is also discussed and compared to that of the free complexes. To the best of our knowledge, this is the first report on the immobilization of Gd-PCTA complexes on dense silica and study of the properties thereof.

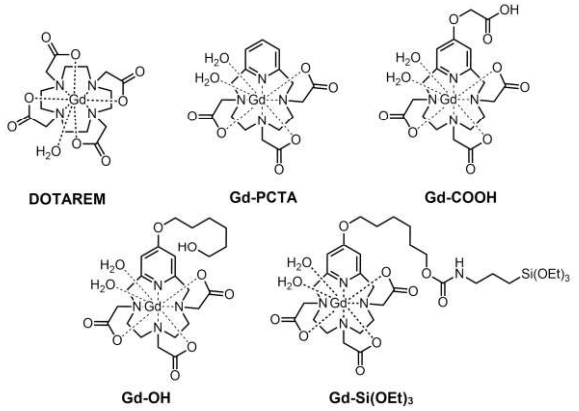

Figure 1 : Structure of the Gd complexes discussed in the text. **Gd-COOH**, **Gd-OH**, **Gd-Si(OEt)$_3$** are new complexes described in this work.

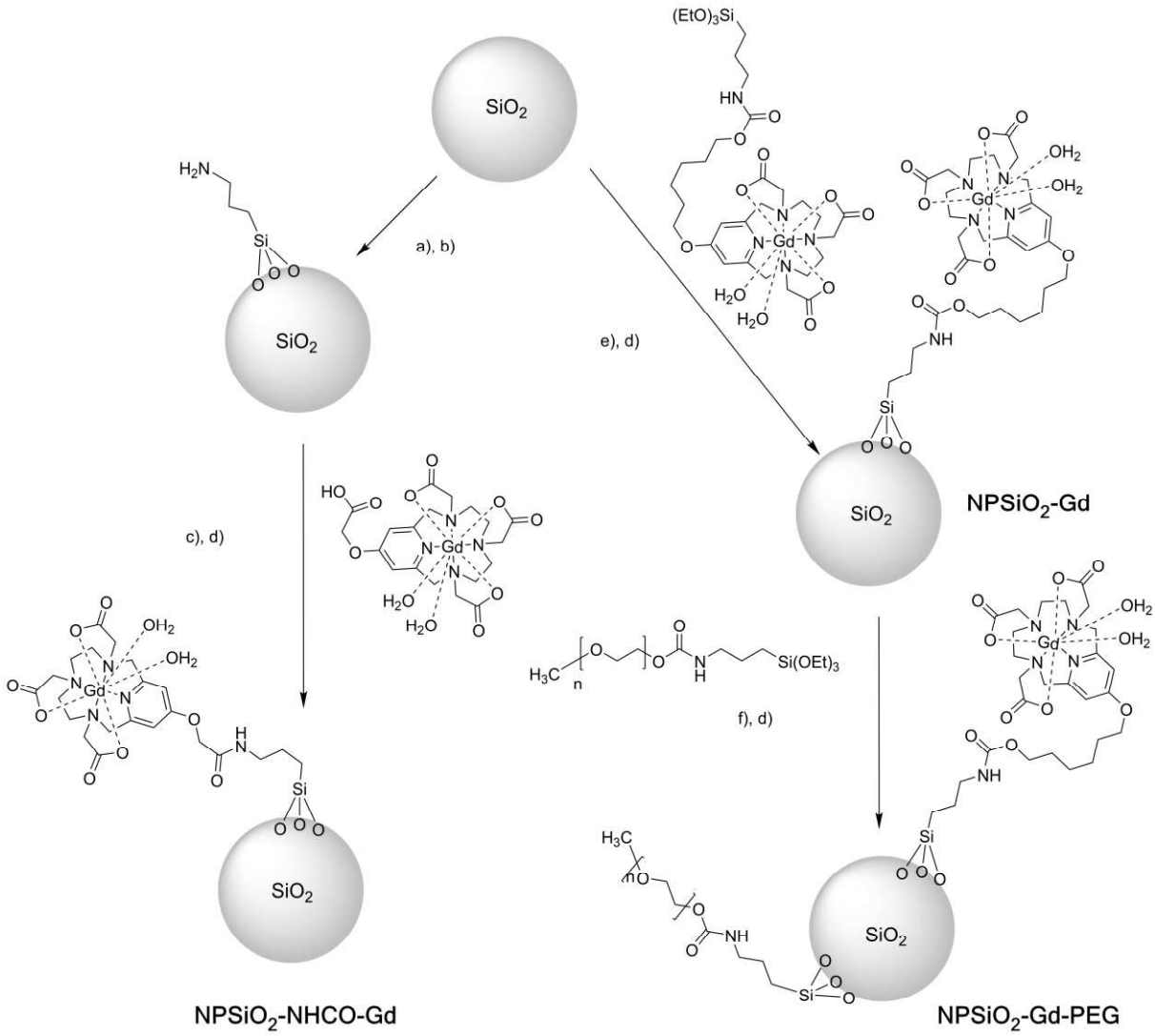

Figure 2 : Amidic coupling strategy (left) and condensation strategy (right). Surface Si-OH functions allowing the condensation of the ethoxy groups have been omitted for clarity ; silica NPs not at scale. *Conditions and reagents* : a) APTMS (excess), r.t., 24h; b) purification by centrifugation with methanol (twice), ethanol (twice), milliQ water (twice) then PBS (10mM, pH=7.4) ; c) PBS (10mM, pH=7.4), Gd-COOH (2q./NH_2), Sulfo-NHS (1.25eq./Gd), EDC (1.25eq./Gd), mixing at 0°C then r.t., 65h; d) purification with milliQ water (4 times) ; e) Gd-$Si(OEt)_3$ (5 eq./nm^2),water/ethanol 1/2(v/v), NH_4OH, 50°C, 48h ; f) PEG-$Si(OEt)_3$ (0.7 eq./nm^2), water/ethanol 1/2(v/v), NH_4OH, 50°C, 48h.

Materials and methods :

Chemicals:

Ethanol (99.9% Aldrich), was dried over magnesium and distilled prior use. DMF (99.8% Aldrich), was dried on molecular sieves and degassed with three freeze pump cycle. Pentane was obtained and purified from a purification MBraun SPS-800 machine and degassed with three freeze-pump cycles. Chelidamic acid (97%, Aldrich), *t*Bu bromoacetate (98%, Alfa Aesar), thionyl chloride (99.5%, Acros Organics), sodium borohydride (98%+ , Acros Organics), calcium chloride (98%, Aldrich), N-bromosuccinimide (99%, Aldrich), triphenylphosphine (99%, Acros Organics), diisopropyl azodicarboxylate (98%, Aldrich), *p*-

toluenesulfonyl chloride (98%, Alfa Aesar), silver oxide (99%, Aldrich), potassium iodide (99%+, Acros Organics), gadolinium chloride hexahydrate (99.999%, Aldrich), ammonia solution (28.0-30%, SigmaAldrich), and 3-(triethoxysilyl)propylisocyanate (TESPIC, Alfa Aesar), Igepal CO-520 (90%, Aldrich), N-hydroxysulfosuccinimide sodium salt (98%+, Aldrich), N-(3-Dimethylaminopropyl)-N'-ethylcarbodiimide hydrochloride (99%+, Aldrich) and aminopropyl trimethoxysilane (Aldrich) were used as received. MilliQ water (18 MΩ) was used for all aqueous preparations, and phosphate buffer solutions (10 mM, pH = 7.4) were prepared a few hours before use. Compounds **1**[20], **2a**[21] and 6-((*tert*-butyldiphenylsilyl)oxy)hexan-1-ol (**$HO(CH_2)_6OSiPh_2tBu$**)[22] were prepared in 74%, 81% and 86% yield respectively, as previously described. The synthesis and characterization of pure silica NPs (**$NPSiO_2$**) were reported in[23]. Functionalization of these NPs with pendant NH_2 functions was carried out and inspired by an already described procedure[24] leading to **$NPSiO_2$-NH_2**. The main features of these starting nanomaterials (**solution 1** - **solution 2**, and **solution 3** respectively) are described in ESI (Figures ESI1-3).

Synthesis of the functionalized PCTA ligands:

Diethyl 4-hydroxypyridine-2,6-dicarboxylate (2b). To a solution of chelidamic acid (1 g, 5 mmol) in absolute ethanol (20 mL) was slowly added thionyl chloride (1 mL, 13.7 mmol). The solution was heated at reflux for 6h. The solvent was evaporated then CH_2Cl_2 (40 mL) and a 10% $NaHCO_3$ solution (5 mL) was added. The organic phase was washed twice with H_2O (2 x 20 mL), dried on $MgSO_4$ and concentrated under reduced pressure. The crude product was purified by column chromatography (SiO_2, CH_2Cl_2/AcOEt, 80/20 then 50/50) to give **2b** as white crystals (0.92 g, 77%). ^{1}H NMR (300 MHz, $CDCl_3$): δ (ppm) = 7.35 (s, 2H), 4.50 (q, *J* = 7.1 Hz, 4H), 1.45 (t, *J* = 7.1 Hz, 6H).

Dimethyl 4-(2-(*tert*-butoxy)-2-oxoethoxy)pyridine-2,6-dicarboxylate (3). The mixture of **2a** (1g, 4.73 mmol) and potassium carbonate (1.03 g, 7.45 mmol) in anhydrous acetonitrile (36 mL) was refluxed 2h under argon atmosphere. *t*Bu bromoacetate (924 mg, 4.73 mmol) was added and the mixture was stirred and heated to reflux 16h. After filtration, the crude mixture was concentrated under reduced pressure and purified by column chromatography (Al_2O_3, CH_2Cl_2/petroleum ether, 10/90) to afford **3** as a pale yellow solid (1.40 g, 90%). ^{1}H NMR (300 MHz, $CDCl_3$): δ= 7.78 (s, 2H), 4.68 (s, 2H), 3.99 (s, 6H), 1.47(s, 9H). ^{13}C NMR (75 MHz, $CDCl_3$): δ= 166.1 (C*q*), 166.0 (C*q*), 164.9 (C*q*), 149.8 (C*q*), 114.5 (CH), 83.5 (C*q*), 65.2 (CH_2), 53.2 (CH_3), 27.9 (CH_3).

***tert*-butyl 2-((2,6-bis(hydroxymethyl)pyridine-4-yl)oxy)acetate (4).** To a solution of **3** (100 mg, 0.31 mmol) in ethanol (7 mL) at 0°C, $CaCl_2$ (103 mg, 0.92 mmol) and sodium borohydride (35 mg, 0.92 mmol) were added gradually. The mixture was stirred 4h and then water (5mL) was added. Ethanol was evaporated and the aqueous phase brought to pH 7 with 1N HCl, and was then extracted with dichloromethane (3x10 mL). The organic layer was dried over anhydrous $MgSO_4$ and the filtrate was concentrated under reduced pressure to afford **4** as a white solid (67 mg, 80%). ^{1}H NMR (300 MHz, $CDCl_3$): δ= 6.70 (s, 2H), 4.69 (s, 4H), 4.57 (s, 2H), 1.48 (s, 9H). ^{13}C NMR (75 MHz, $CDCl_3$): δ= 166.8 (C*q*), 165.5 (C*q*), 160.5 (C*q*), 105.4 (CH), 83.1 (C*q*), 65.1 (CH_2), 64.4 (CH_2), 28.0 (CH_3).

***tert*-butyl 2-((2,6-bis(bromomethyl)pyridine-4-yl)oxy)acetate (5).** To a solution of **4** (723 mg, 2.69 mmol) and PPh_3 (1.833 g, 6.99 mmol) in dry CH_2Cl_2 (30 mL) at 0°C under argon

atmosphere, NBS (1.244 g, 6.991 mmol) was added gradually (in 4 times) and the mixture was stirred for 90 minutes at room temperature. The mixture was concentrated to dryness. The pale yellow solid obtained (4.17 g) was purified by column chromatography (SiO_2, CH_2Cl_2) to afford **5** as a white solid (775 mg, 73%). ^{1}H NMR (300 MHz, $CDCl_3$): δ= 6.87 (s, 2H), 4.58 (s, 2H), 4.46 (s, 4H), 1.49 (s, 9H). ^{13}C NMR (75 MHz, $CDCl_3$): δ= 166.6 (C*q*), 165.7 (C*q*), 158.3 (C*q*), 109.3 (CH), 83.3 (C*q*), 65.3 (CH_2), 33.4 (CH_2), 28.1 (CH_3).

Diethyl 4-((6-((*tert*-butyldiphenylsilyl)oxy)hexyl)oxy)pyridine-2,6-dicarboxylate (6). A solution of **2b** (500 mg, 2.09 mmol) in anhydrous THF (48 mL) was placed under argon atmosphere. **$HO(CH_2)_6OSiPh_2tBu$** (1.53g, 4.31 mmol) dissolved in THF (12 mL) and triphenylphosphine (1.13 g, 4.31 mmol) were added and the mixture was stirred until a homogeneous solution was obtained. DIAD (0.82 mL, 4.18 mmol) was added drop by drop and the mixture was heated to reflux and stirred overnight under argon atmosphere. After concentration under reduced pressure, the residue was purified by column chromatography (SiO_2, petroleum ether/AcOEt, 80/20) to afford **6** as a colorless oil (1.12 g, 93%). ^{1}H NMR (300 MHz, $CDCl_3$): δ= 7.76 (s, 2H), 7.69 – 7.65 (m, 4H), 7.44 – 7.34 (m, 6H), 4.47 (q, *J* = 7.2 Hz, 4H), 4.10 (t, *J* = 6.4 Hz, 2H), 3.67 (t, *J* = 6.3 Hz, 2H), 1.86 – 1.77 (m, *J* = 6.5 Hz, 2H), 1.62 – 1.55 (m, 2H), 1.45 (m, 10H), 1.04 (s, 9H). ^{13}C NMR (75 MHz, $CDCl_3$): δ= 167.0 (C*q*), 164.7 (C*q*), 150.1 (C*q*), 135.5 (CH), 134.0 (C*q*), 129.5 (CH), 127.5 (CH), 114.3 (CH), 68.9 (CH_2), 63.7 (CH_2), 62.3 (CH_2), 32.3 (CH_2), 28.7 (C*q*), 26.8 (CH_3), 25.5 (CH_2), 25.4 (CH_2), 19.2 (CH_2), 14.2 (CH_3).

(4-((6-((*tert*-butyldiphenylsilyl)oxy)hexyl)oxy)pyridine-2,6-diyl)dimethanol (7). To a solution of **6** (760 mg, 1.31 mmol) in ethanol (95 mL) at 0°C, $CaCl_2$ (440 mg, 3.95 mmol) and sodium borohydride (150 mg, 3.95 mmol) were added gradually. The mixture was stirred 4h and then water (30 mL) was added. Ethanol was evaporated and the aqueous phase brought to pH 7 with 1N HCl was extracted with dichloromethane (3x30 mL). The organic layer was dried over anhydrous $MgSO_4$ and the filtrate was concentrated under reduced pressure and purified by column chromatography (Al_2O_3, CH_2Cl_2/MeOH, 97/3) to afford **7** as a white solid (525 mg, 81%). ^{1}H NMR (300 MHz, $CDCl_3$): δ= 7.69 – 7.65 (m, 4H), 7.45 – 7.40-7.37 (m, 6H), 6.69 (s, 2H), 4.67 (s, 4H), 3.99 (t, *J* = 6.5 Hz, 2H), 3.67 (t, *J* = 6.3 Hz, 2H), 1.82-1.73 (m, 2H), 1.63-1.55 (m, 2H), 1.45-1.41 (m, 4H), 1.05 (s, 9H). ^{13}C NMR (75 MHz, $CDCl_3$): δ= 166.6 (C*q*), 160.3 (C*q*), 135.5 (CH), 134.0 (C*q*), 129.5 (CH), 127.6 (CH), 105.6 (CH), 68.1 (CH_2), 64.4 (CH_2), 63.7 (CH_2), 32.3 (CH_2), 28.8 (C*q*), 26.8 (CH_3), 25.6 (CH_2), 25.5 (CH_2), 19.2 (CH_2). MS (ESI^+): m/z, 494.3 $[M+H]^+$ (100%).

(4-((6-((*tert*-butyldiphenylsilyl)oxy)hexyl)oxy)pyridine-2,6-diyl)bis(methylene)bis(4-methylbenzenesulfonate) (8). A mixture of **7** (80 mg, 0.16 mmol), potassium iodide (11 mg, 66 µmol) and silver oxide (113 mg, 0.49 mmol) in anhydrous dichloromethane (3.5 mL) was stirred at -20°C under argon atmosphere. *p*-Toluenesulfonyl chloride (62 mg, 0.32 mmol) was then added and the mixture was stirred overnight at room temperature under argon atmosphere. After Celite filtration and washing with dichloromethane, the filtrate was concentrated under reduced pressure and purified by column chromatography (Al_2O_3, AcOEt/petroleum ether, 10/90) to afford **8** as a colorless oil (110 mg, 87%). ^{1}H NMR (300 MHz, $CDCl_3$): δ= 7.85 – 7.82 (m, 4H), 7.70 – 7.66 (m, 4H), 7.46 – 7.26 (m, 10H), 6.79 (s, 2H), 4.97 (s, 4H), 3.93 (t, *J* = 6.4 Hz, 2H), 3.69 (t, *J* = 6.3 Hz, 2H), 2.43 (s, 6H), 1.79 – 1.71 (m, 2H), 1.63 – 1.56 (m, 2H), 1.45 – 1.40 (m, 4H), 1.05 (s, 9H). ^{13}C NMR (75 MHz, $CDCl_3$): δ= 166.8 (C*q*),

155.0 (C*q*), 145.1 (Cq), 135.5 (CH), 134.0 (C*q*), 132.7 (C*q*), 129.9 (CH), 129.5 (CH), 128.0 (CH), 127.6 (CH), 107.6 (CH), 71.2 (CH_2), 68.4 (CH_2), 63.7 (CH_2), 32.4 (CH_2), 28.8 (C*q*), 26.9 (CH_3), 25.6 (CH_2), 25.5 (CH_2), 21.6 (CH_3), 19.2 (CH_2).

Compound 9. The mixture of **1** (289 mg, 0.646 mmol) and sodium carbonate (690 mg, 6.46 mmol) in anhydrous acetonitrile (300 mL) was refluxed for 90 minutes under argon atmosphere. A solution of **5** (256 mg, 0.646 mmol) in anhydrous acetonitrile (30 mL) was added and the mixture was stirred and heated to reflux 16h under argon atmosphere. After filtration, the filtrate was concentrated under reduced pressure and purified by column chromatography (Al_2O_2, CH_2Cl_2/MeOH, 100/0 then 98/2). The first recovered fraction was a mixture of the macrocycle in its free form and its sodium salt form (sodium adduct) while in the second recovered fraction, only the sodium adduct was obtained. However, subsequent treatment of both fractions by a saturated aqueous solution of EDTA to remove sodium species afforded **9** as a yellow oil (285 mg, 65%).

Sodium adduct : ^{1}H NMR (300 MHz, $CDCl_3$): δ= 6.61 (s, 2H), 4.57 (s, 2H), 4.02 (d, J_{AB} = 15 Hz, 2H), 3.61 (d, J_{AB} = 15 Hz, 2H), 3.48 (d, J_{AB} = 17.5 Hz, 2H), 3.38 (d, J_{AB} = 17.5 Hz, 2H), 3.05 (s, 2H), 2.60-2.40 (m, 4H), 2.20-1.80 (m, 2H), 1.84-2.04 (m, 2H), 1.46 (s, 9H), 1.44 (s, 18 H), 1.42 (s, 9H).^{13}C NMR (75 MHz, $CDCl_3$): δ= 172.8 (C*q*), 172.4 (C*q*), 166.8 (C*q*), 165.6 (C*q*), 160.0 (C*q*), 107.7 (CH), 82.9 (C*q*), 82.1 (C*q*), 82.1 (C*q*), 65.2 (CH_2), 62.1 (CH_2), 59.2 (CH_2), 55.7 (CH_2), 53.8 (CH_2), 52.9 (CH_2), 28.1 (CH_3), 27,9 (CH_3), 27,8 (CH_3).

Free form : ^{1}H NMR (300 MHz, $CDCl_3$): δ= 6.67 (s, 2H), 4.55 (s, 2H), 3.96 (s, 4H), 3.40 (s, 4H), 3.1-3.35 (m, 2 H), 2.25-3.0 (m, 8 H), 1.47 (s, 9H), 1.46 (s, 18H), 1.41 (s, 9H).^{13}C NMR (75 MHz, $CDCl_3$): δ= 170.6 (C*q*), 166.8 (C*q*), 165.4 (C*q*), 159.5 (C*q*), 108.7 (CH), 82.9 (C*q*), 81.2 (C*q*), 81.1 (C*q*), 65.1 (CH_2), 59.9 (CH_2), 58.3 (CH_2), 55.7 (CH_2), 50.4 (CH_2), 50.1 (CH_2), 28.1 (CH_3), 28.0 (CH_3), 27.9 (CH_3). MS (ESI^+): m/z 455.2 $[M\text{-}4tBu+5H]^+$ (18%), 511.2 $[M\text{-}3tBu+4H]^+$ (35%), 567.3 $[M\text{-}2tBu+3H]^+$ (64%), 623.3 $[M\text{-}tBu+2H]^+$ (76%), 679.4 $[M+H]^+$ (100%), 701.4 $[M+Na]^+$ (22%). HRMS (ESI^+): m/z calcd for $C_{35}H_{59}N_4O_9$ $[M+H]^+$ 679.4282 found 679.4282.

Compound 10. A solution of **9** (69 mg, 0.1 mmol) in an equivolumic mixture of 2N HCl solution (3 mL) and dichloromethane (3 mL) was stirred 16 h at room temperature. The organic layer was isolated and the aqueous layer was concentrated under reduced pressure to afford **10** as a white solid (45 mg, 100%). ^{1}H NMR (300 MHz, D_2O, Figure ESI4): δ= 7.15 (s, 2H), 4.92 (s, 2H), 4.56 (s, 4H), 4.07 (s, 4H), 3.85 (s, 2H), 3.40-2.70 (m, 8H). ^{13}C NMR (75 MHz, D_2O, Figure ESI5): δ= 171.9 (C*q*), 171.6 (C*q*), 171.2 (C*q*), 168.7 (C*q*), 152.7 (C*q*), 109.7 (CH_2), 65.6 (CH_2), 58.4 (CH_2), 56.3 (CH_2), 54.4 (CH_2), 52.42 (CH_2), 52.38 (CH_2). MS (ESI^+): m/z 455.1 $[M+H]^+$ (100%), 477.1 $[M+Na]^+$ (28%). HRMS (ESI^+): m/z calcd for $C_{19}H_{27}N_4O_9$ $[M+H]^+$ 455.1778 found 455.1781. Elemental Analysis calculated for $C_{19}H_{26}N_4O_9.4HCl.3H_2O$: C, 34.88, H, 5.55, N, 8.56. Found C, 34.93, H, 5.74, N, 8.53.

Compound 11. The mixture of **1** (65 mg, 0.14 mmol) and sodium carbonate (145 mg, 1.37 mmol) in anhydrous acetonitrile (50 mL) was heated 30 minutes to reflux under argon atmosphere. A solution of **8** (110 mg, 0.14 mmol) in anhydrous acetonitrile (20 mL) was added and the mixture was stirred and heated to reflux 16 h under argon atmosphere. After filtration, the filtrate was concentrated to dryness and purified by column chromatography (Al_2O_3, CH_2Cl_2/MeOH, 98/2) to afford **11** as a yellow oil (95 mg, 75%). ^{1}H NMR (300 MHz, $CDCl_3$): δ= 7.65 – 7.62 (m, 4H), 7.42 – 7.32 (m, 6H), 6.62 (s, 2H), 3.98 (t, *J* = 6.4 Hz, 2H), 3.95

(d, J_{AX} = 14.2 Hz, 2H), 3.64 (t, J = 6.3 Hz, 2H), 3.53 (d, J_{AX} = 14.2 Hz), 3.45 (d, J_{AB}= 14.2 Hz, 2H), 3.32 (d, J_{AB}= 14.2 Hz, 2H), 3.09 (s, 2H), 2.55 (t, J = 5.2 Hz, 4H), 2.15 (m, 2H,), 1.97 – 1.88 (m, 2H), 1.79 - 1.70 (m, 2H), 1.61 – 1.52 (m, 2H), 1.45 (m, 31H), 1.02 (s, 9H). ^{13}C NMR (75 MHz, $CDCl_3$): δ= 173.3 (C*q*), 172.8 (C*q*), 166.9 (C*q*), 159.4 (C*q*), 135.4 (CH), 133.9 (C*q*), 129.4 (CH), 127.5 (CH), 108.1 (CH), 82.7 (C*q*), 82.4 (C*q*), 68.4 (CH_2), 63.7 (CH_2), 62.4 (CH_2), 59.3 (CH_2), 55.9 (CH_2), 53.5 (CH_2), 53.0 (CH_2), 32.3 (CH_2), 28.7 (CH_2), 27.9 (CH_3), 27.8 (CH_3), 26.8 (CH_3), 25.6 (CH_2), 25.4 (CH_2), 19.1 (Cq). HRMS (ESI$^+$): m/z calcd for $C_{51}H_{79}N_4O_8Si$, 100% $[M+H]^+$ 903.5667 found 903.5688.

Compound 12. A solution of **11** (69 mg, 76 µmol) in an equivolumic mixture of 6N HCl solution (3 mL) and dichloromethane (3 mL) was stirred and heated to reflux overnight. The organic layer was isolated and the aqueous layer was concentrated under reduced pressure to afford **12** as a yellowish oil (40 mg, 82%). ^{1}H NMR (300 MHz, D_2O, Figure ESI6): δ =7.15 (s, 2H), 4.41 (s, 4H), 4.23 (t, J = 6.3 Hz, 2H), 4.04 (s, 2H), 3.93 (s, 4H), 3.52 (t, J = 6.5 Hz, 2H), 3.23 (s, 8H), 1.81 – 1.73 (m, 2H), 1.51 – 1.31 (m, 6H). ^{13}C NMR (75 MHz, D_2O, Figure ESI7): δ= 173.5 (C*q*), 171.4 (C*q*), 170.2 (C*q*), 152.8 (C*q*), 109.9 (CH), 70.9 (CH_2), 61.7 (CH_2), 57.7 (CH_2), 56.3 (CH_2), 54.6 (CH_2), 53.5 (CH_2), 50.8 (CH_2), 31.1 (CH_2), 27.7 (CH_2), 24.7 (CH_2), 24.6 (CH_2). HRMS (ESI$^+$): m/z calcd for $C_{23}H_{37}N_4O_8$, 100% $[M+H]^+$ 497.2611 found 497.2617. Elemental Analysis calculated for $C_{23}H_{36}N_4O_8$.4 HCl.2.25 H_2O: C, 40.55, H, 6.51, N, 8.22. Found C, 40.65, H, 5.68, N, 8.16.

Complexation of Gd ions

Gd-COOH. A mixture of **10** (65 mg, 99 µmol) and gadolinium(III) chloride hexahydrate (38 mg, 108 µmol) in water (5mL) was stirred 1h at room temperature. pH was adjusted to 5-6 with a solution of sodium hydroxide (0.1N) added 50µL by 50µL then the mixture was stirred overnight at room temperature. pH was adjusted to 7 and the solution was purified using a SEP PAK C18 column. Each fraction was analyzed in UV-Vis absorption (blank H_2O) and fractions with gadolinium complex were brought together and concentrated under reduced pressure to afford **Gd-COOH** as a yellowish glittery solid (55 mg, 88%). HRMS (ESI$^+$, Figure ESI8): m/z calcd for $C_{19}H_{24}GdN_4O_9$, 100% $[M+H]^+$ 610.0789 found 610.0790

Gd-OH. A mixture of **12** (33 mg, 48.3 µmol) and gadolinium(III) chloride hexahydrate (23 mg, 62 µmol) in water (1-2mL) was stirred 1h at room temperature. pH was adjusted to 5-6 with a solution of sodium hydroxide (0.1N) added 50 µL by 50 µL then the mixture was stirred overnight at room temperature. pH was adjusted to 7 and the solution was purified using a SEP PAK C18 column. Each fraction was analyzed in UV-Vis absorption (blank H_2O) and fractions with gadolinium complex are brought together and concentrated to dryness to afford **Gd-OH** as a yellowish glittery solid (24 mg, 76%). HRMS (ESI$^+$, Figure ESI9): m/z calcd for $C_{23}H_{34}GdN_4O_8$, 100% $[M+H]^+$ 652.1623 found 652.1628

Gd-Si(OEt)$_3$ *:* Proton exchange reaction between **Gd-OH** and TESPIC was adapted from[25] as follows. **Gd-OH** was lyophilized beforehand. 34 mg (50 µmol) of **Gd-OH** was dissolved in 5 mL of dried DMF (<10 ppm H_2O). Then, 12 µL of TESPIC (45 µmol, 0.9 eq.), were added and the mixture was heated at 70°C for four days. The solvent was removed under reduced pressure at 70°C and the residue washed three times with 2mL of dry pentane (<5 ppm H_2O), and finally dried under reduced pressure at room temperature to yield **Gd-Si(OEt)$_3$** as a pale

yellow powder (yield 70%). IR-ATR: ν(C=O urethane) = 1707 cm^{-1}, ν(Si-O) = 1070 cm^{-1}, ν($\underline{CH_3}$-CH_2-O-Si) = 2972 cm^{-1}).

*Grafting of **Gd-COOH** on **$NPSiO_2$-NH_2** (synthesis of **$NPSiO_2$-NHCO-Gd**):*

Solution 3 (around 100mg of **$NPSiO_2$-NH_2** corresponding to around 10 µmol of free NH_2 groups in solution see ESI) was put in an ice bath at 0°C. In a pyrex tube, 12.9 mg (20 µmol, 2 eq. of Gd per accessible NH_2 surface group) of **Gd-COOH** were dissolved in 5 mL of PBS 10 mM (pH = 7.4) with 1 minute of sonication bath. The solution was then put in an ice bath (0°C). Two stock solutions of N-hydroxysulfosuccinimide sodium salt (Sulfo-NHS) and N-(3-Dimethylaminopropyl)-N'-ethylcarbodiimide hydrochloride (EDC) were prepared in PBS (pH=7.43, 10mM) at a concentration of 100 $mg.mL^{-1}$. Addition of 55µL of the Sulfo-NHS solution (5.5 mg, 25µmol) to the **Gd-COOH** solution was followed by 30 seconds of vortexing at 0°C. Then 48.5 µL of the EDC (4.85 mg, 25 µmol) solution were added and the mixture was vortexed for 30 seconds at 0°C. Then the solution containing the **$NPSiO_2$-NH_2** was added at 0°C, and the final solution was vortexed for 30 seconds then put under mechanical stirring at r.t. for 65 hours. The solution was then washed four times with milliQ water (9000 rpm, 30 minutes, 15°C, Vortex 1 min, sonication bath 5 minutes), and the final product redispersed in 10mL of milliQ water.(% Gd = 0.35 w% in the powder obtained after lyophilization).

In a control experiment, this process was repeated in the absence of Sulfo-NHS and EDC, while maintaining all other parameters constant.

*Grafting of **Gd-Si(OEt)$_3$** on **$NPSiO_2$** (synthesis of **$NPSiO_2$-Gd**) adapted from[25]:* 5 mL of absolute ethanol were added to **solution 2** (a 10 mL dispersion of the silica NPs in milliQ water was obtained [$NPSiO_2$]≅ 2.5 $mg.mL^{-1}$ as described in ESI) to yield a 2:1 ratio v/v solution (milliQ water:ethanol). Addition of 12 mg (12.7 µmol) of **Gd-Si(OEt)$_3$** was followed by a 10 minutes sonication of the mixture. Then, 0.325 mL of 30% (w%) NH_4OH were added to the mixture which was then heated at 50°C for 48 hours without stirring. The particles were then washed 4 times with 10 mL of milliQ water (Vortex 1 min, sonication 5 minutes, centrifugation 1 hour 30 minutes, 12000 rpm, 15°C). The NPs were dispersed in 10mL of milliQ water (**Solution 4**). [$NPSiO_2$-Gd] = 1.8 mg/mL^{-1} and %Gd = 0.9w% in the powder obtained after lyophilization. The dried powder was analyzed by DRIFT ν(C=O urethane) = 1703 cm^{-1}, ν(Si-O-Si) = 1093 cm^{-1}, ν (aliphatic chains) = 2966 - 2870 cm^{-1}.

*Pegylation (synthesis of **$NPSiO_2$-Gd-PEG**) adapted from a previous publication[23]*: 5 mL of absolute ethanol was added to **solution 4** to yield a 2:1 ratio v/v solution (MilliQ water:ethanol). Addition of 25 mg of previously synthesized PEG-silane was followed by a 10 minutes sonication of the mixture. Then, 0.325 mL of 30% NH_4OH was added to the mixture, which was then heated at 50°C for 48 hours without stirring. The particles were then washed 4 times with 10 mL of MilliQ water (Vortex 1 min, sonication 5 minutes, centrifugation 1 hour 30 minutes, 12000 rpm, 15°C). The NPs were redispersed in 10 mL of MilliQ water. [$NPSiO_2$-Gd-PEG] = 1.2 $mg.mL^{-1}$; %C = 4.68; %H= 1.31; %N= 0.35; %Gd = 0.7 (w%) in the powder obtained after lyophilization). The dried powder was analyzed by DRIFT ν(C=O urethane) = 1710 cm^{-1}, ν(Si-O-Si) = 1093 cm^{-1}, ν (aliphatic chains) = 2966 - 2855 cm^{-1}.

<u>Characterizations:</u>

Gadolinium content in the samples was determined by inductively coupled plasma-optical emission spectrometry (ICP-OES, PerkinElmer Optima 2100 DV ICP), after digesting the samples into a mixture of HNO_3: HCl (1:3 ratio v/v) and diluting them with ultrapure water.

C, H and N contents were determined on a PERKIN ELMER 2400 série II simultaneous CHN elemental analyzer (ThermoScientific).

FT-IR spectra were recorded in ATR mode on a Bruker Alpha FT-IR spectrophotometer placed in the glove box for air sensitive samples and on a PerkinElmer Frontier FT-IR spectrophotometer for air stable samples. Diffuse reflectance infrared Fourier transform (DRIFT) spectra were acquired on a Nexus Nicolet with a DRIFT accessory from Perkin Elmer with a resolution of 0.8 cm^{-1} and a deuterated triglycine sulfate (DTGS) detector. All spectra were recorded in solid state after lyophilization of the samples.

^{1}H and ^{13}C NMR spectra were recorded using a Bruker Avance 300 spectrometer (300 MHz for ^{1}H and 75 MHz for ^{13}C). Chemical shifts are reported in ppm, with residual protonated solvents as the internal references.

Electrospray (ESI) mass spectra were obtained on a Q TRAP Applied Biosystems spectrometer and *High-Resolution Mass Spectra* (HRMS) on a Xevo G2 QTof Waters spectrometer.

Fluorescence measurements for the titration of free NH_2 groups were performed on a Horiba Jobin Yvon FluoroMax®-4 spectrofluorometer according to [26]. Emission spectra and luminescence decays at room temperature of europium complexes were measured using a Cary Eclipse spectrofluorimeter equipped with a Xenon flash lamp source and a Hamamatsu R928 photomultiplier. Lifetimes (uncertainty ≤ 5%) are made by monitoring the decay at a wavelength corresponding to the maximum intensity of the emission spectrum, following pulsed excitation.

Transmission electron microscopy (TEM) samples were prepared by the drop casting method on copper grids coated with a carbon film. TEM images were recorded on MET Jeol JEM 1011 or 1400 instruments, size distributions were acquired by measuring a minimum of 250 objects using the open source ImageJ software. Sizes are given as mean ± standard deviation according to a Gaussian fit of the corresponding size distribution. EDX study was performed on a MET Jeol JEM 2100F instrument. Atom resolved images have been obtained on a probe-corrected cold FEG MET Jeol JEM-ARM200F.

The hydrodynamic sizes (DHYD) were measured by dynamic light scattering (DLS), using a Zetasizer NanoZ device (Malvern instruments). Dilute suspensions were prepared in milliQ water (10^{-5} mol/L). The solutions were filtrated on a cellulose 0.450 µm filter before analysis. DHYD in this work refers to the Z-average diameter.

The Zeta potential study was performed, using a Zetasizer NanoZ device (Malvern instruments). Two stock solutions were prepared for each sample, one for the study in basic pH and one for the study in acidic pH. The pH was adjusted with 0.001mol.L^{-1} and 0.01 mol.L^{-1} HCl and NaOH solutions in order to keep the dilution of the NPs the same for each measurement. Samples were analyzed from pH=1 to pH=12.

To evaluate the efficiency of the hydrophilic suspensions of the monomeric complexes and of the complexes grafted on the silica nanoparticles as MRI contrast agents, *T_2 and T_1*

relaxation times were measured with a Minispec MQ60 (Bruker) operating at 37°C and 60MHz, with a magnetic field of 1.5T and a Minispec MQ20 (Bruker) operating at 37°C and 20MHz with a magnetic field of 0.47T. The *relaxation rate Ri values* ($1/T_i$, s^{-1}, i=1,2), obtained from the relaxation times measured (T_i, s), were corrected by subtracting the water relaxation rate ($R(H_2O)$ = 0.2826 s^{-1} at 37°C) in the absence of the contrast agent for the monomeric complexes, or in the presence of ungrafted silica nanoparticles for the nanoparticulate ones (R_1 = 0.34 s^{-1} at 20 MHz and 37°C, and R_1 = 0.31 s^{-1} at 60 MHz and 37°C). Linear fitting of the data gives straight lines whose slopes are the relaxivities (r_i, $s^{-1}.mmol^{-1}$, with $R^2 > 0.99$) related to the gadolinium concentration ($mmol.L^{-1}$). *Nuclear magnetic relaxation dispersion (NMRD) profiles* were recorded at 37°C on a field cycling relaxometer (Stelar, Italy) at magnetic fields ranging from 4.7 10^{-4} (0.02 MHz) to 0.94 T (40 MHz). The fitting of the data was performed according to the Solomon and Bloembergen model (SBM) [27–29] using a home-made fitting program. To fit the data we fixed the average water-Gd(III) distance *d* to *d = 0.36 nm.* The water diffusion coefficient was fixed at $D = 3.3.10^{-9}\ m^2.s^{-1}$, the distance between the coordinated water molecules and the Gd(III) ion *r* at 0.31 nm, and τ_M (residence time of water in the first coordination sphere) at 100 ns [30]. The number of hydration q was taken as 2 on the basis of fluorescence measurements made on Eu(III) analogues of the complexes by determining their luminescence lifetimes in H_2O and D_2O solutions and using the phenomenological Supkowski and Horrocks equation[31]. For example, a q value of 2.04 for Eu-COOH was calculated from lifetimes of this complex in H_2O (0.38 ms) and D_2O (2.07 ms). For the Gd-complexes grafted on silica NPs (samples **$NPSiO_2$-Gd** and **$NPSiO_2$-Gd-PEG**), the diamagnetic contribution of silica (determined from an independent measurement on **$NPSiO_2$** taken as a reference) has been subtracted and only the higher field part of the NMRD profile was fitted because the SBM theory does not allow to fit correctly the whole profile. *Phantom samples* were prepared in 250 μL eppendorfs by diluting the samples with pure water to afford the expected concentration range, images were acquired on a Biospec 9.4T MRI from Bruker and on an ICON 1T from Bruker. At 9.4T, a RARE (Rapid Acquisition with Relaxation Enhancement) sequence with variable repetition time (TR, allowing for T_1 measurement via saturation-recuperation method) was used (TR were 54.426; 100; 250; 500; 750; 1000; 1500; 3000; 4500; 6000; 8000; 10000; 15000; 20000 ms. Other parameters were TE=10 ms, NEX=1, RARE factor: 2, slice thickness: 1.25 mm, resolution: 312x312 microns). Images obtained at TR= 250ms were selected to illustrate T_1 effect of compounds at 9.4T. At 1T, a T_1-weighted RARE sequence with the following parameters was used: TR: 500 ms, TE: 8 ms, NEX: 4, RARE factor: 1, slice thickness: 1.25 mm, resolution: 312x312 microns.

Toxicity assessments: Human colorectal carcinoma cells (HCT 116) were obtained from American Type Culture Collection (ATCC CCL-247) and Human transformed skin fibroblasts (1BR3G) were obtained from European Collection of Authenticated Cell Cultures (ECACC 90020507). Both cell lines were routinely cultured in Dulbecco's Modified Eagle Medium (DMEM, Invitrogen) containing 10% heat-inactivated fetal bovine serum at 37°C in a humidified 10% CO_2 atmosphere. The cytotoxicity of each sample was evaluated using Resazurin sodium salt (Sigma-Aldrich) in DBPS (Gibco) at 0.15 mg/ml. Stock solutions for NPs were prepared in milliQ Water. All working concentrations were prepared in DMEM medium with a maximum of 10% of milliQ water in all working concentrations. Cells were plated in

96-well plates at a density of 5 × 10^3 cells/well in 100 µL of culture medium and were allowed to grow overnight. After this time, cells were treated with different dilutions (0, 10, 20, 50, 100, or 200 times) of each samples during 24 h and 72 h and then 10 µL of Resazurin solution reagent was added following the standard protocol[32]. After 3 h incubation, fluorescence was measured exciting at 531 nm (emission at 572 nm) using a Victor3 multiwell microplate reader (Perkin Elmer). The relative cell viability (%) for each sample related to the control cells without treatment was calculated. Each sample was tested in triplicate.

Results

Synthesis of gadolinium (III) complexes derived from PCTA.

The synthetic pathway for the preparation of the two bifunctional PCTA chelates bearing a carboxylic acid (**Gd-COOH**) or a hydroxyl (**Gd-OH**) function is depicted in Figure 3 and is based on our methodology used for the access of PCTA and its bifunctional derivatives.[21,33]

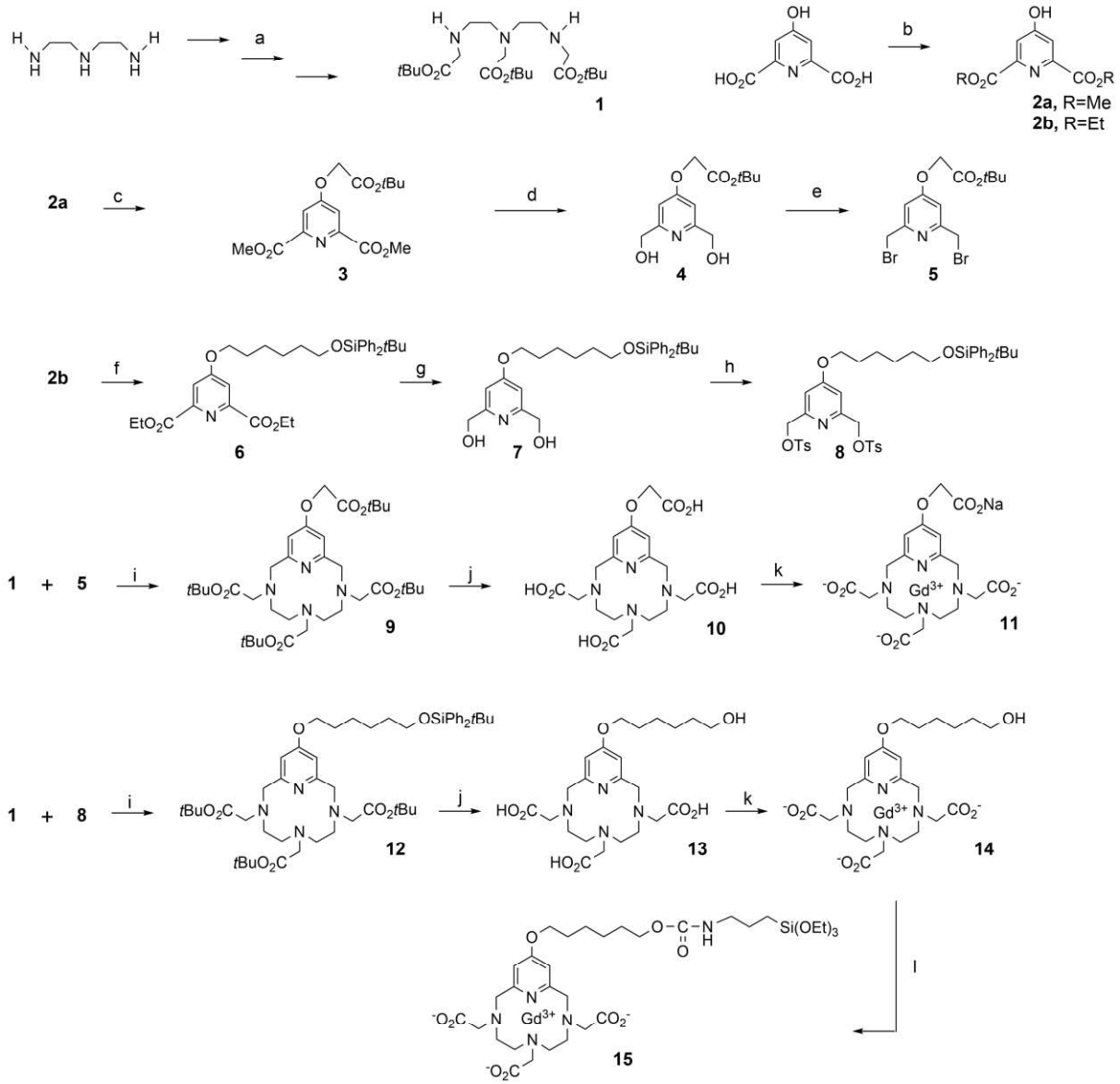

Figure 3: Synthesis of gadolinium(III) complexes derived from PCTA. a) three steps, overall yield 74% [20]; b) **2a**: $SOCl_2$, MeOH, reflux, 6 h, 81% [21]; **2b**: $SOCl_2$, EtOH, reflux, 6 h, 77%; c) $BrCH_2COOtBu$, K_2CO_3, CH_3CN, reflux, 16 h, 90%; d) $NaBH_4$, $CaCl_2$, EtOH, 0°C, 4 h, 80% ; e) NBS, PPh_3, CH_2Cl_2, rt, 1h 30, 73% ; f) **$HO(CH_2)_6OSiPh_2tB$** [22], DIAD, PPh_3, THF, reflux, overnight, 93% ; g) $NaBH_4$, $CaCl_2$, EtOH, 0°C, 4 h, 81% ; h) TsCl, Ag_2O, KI, CH_2Cl_2, -20°C then rt overnight, 87% ; i) [reagents] = 2×10^{-3} M, Na_2CO_3, CH_3CN, reflux 16 h, 65% (**9**), 75% (**11**) ; j) **10**: 2N aqueous HCl/CH_2Cl_2 50/50, rt, 16 h, 100%; **12**: 6N aqueous HCl/CH_2Cl_2 50/50, reflux, overnight, 82% ; k) $GdCl_3.6H_2O$, $NaOH/H_2O$ (pH = 6), rt, overnight, 88% (**Gd-COOH**), 76% (**Gd-OH**) ; l) $OCN(CH_2)_3OSi(OEt)_3$, DMF, 70°C, 96 h, 70%.

The synthetic pathway requires three key compounds: triamine derivative **1** bearing three masked acetate arms and trifunctionalized pyridine derivatives **5** and **8**. The key intermediate **1** was obtained in a three step sequence from diethylenetriamine following our previously reported procedure (overall yield 74%).[20] Starting from commercially available chelidamic acid, the two other synthons were obtained in four steps. Regarding the preparation of dibromo derivative **5**, diol **4** was prepared by a Williamson route *via* a K_2CO_3-promoted coupling reaction between dimethyl chelidamate[21] and *tert*-butyl bromoacetate, followed by a selective reduction of methyl ester groups with sodium borohydride and calcium chloride in ethanol at 0°C. The diol compound was then converted into its dibromide derivative under acid-free conditions by using PPh_3/NBS system. As far as the preparation of the third key intermediate **8** is concerned, bromation of TBDPS monoprotected 1,6-hexanediol and subsequent o-alkylation of diethyl chelidamate afforded the silyl ether-terminated pyridine derivative **6** in 31% yield. Compound **6** could be more conveniently obtained in one step by exploiting the Mitsunobu reaction. Thus, treatment of diethyl chelidamate with monoprotected 1,6-hexanediol in the presence of DIAD and PPh_3 afforded **6** in 93% yield. As functionalization of diol **7** as dibromide by using PPh_3/NBS or PPh_3/CBr_4 systems did not give satisfactory results (yield $<$ 20%), we turned our attention to the preparation of the ditosylate derivative **8**. Among conventional methods to prepare tosyl ester (TsCl/NaOH, $TsCl/NEt_3$, and $TsCl/Ag_2O$ protocols), the treatment of **7** by *p*-toluenesulfonyl chloride in the presence of Ag_2O and KI afforded the best result for this step, **8** being obtained in 87% yield.

The macrocyclization step was attempted using a batchwise procedure and under the control of a metal-ion template effect. Intermolecular cyclization between triamine **1** and bis bromide **5** or bis sulfonate ester **8** derivatives was carried out in acetonitrile at reflux (reagents concentration = 2×10^{-3} M) and in the presence of sodium carbonate. The ^1H NMR analysis of the crude reaction mixture revealed the presence of a major macrocyclic species identified as the Na^+ adduct of the 1:1 cyclization product. Purification of the crude macrocyclisation mixture by column chromatography on alumina and subsequent treatment by a saturated aqueous solution of EDTA to remove sodium species afforded the Na^+-free prochelators **9** and **11** in 65 and 75% yield, respectively. Deprotection of *tert*-butyl esters and silyl-ether groups was achieved in aqueous 2N HCl at room temperature or in 6N HCl at reflux and afforded respectively, polyacids ligands **10** and **12** as their tetrahydrochloride salts in excellent yields (quantitative yield for **10** and 82% for **12**). The corresponding Gd(III) complexes, **Gd-COOH** and **Gd-OH**, were prepared at room temperature by mixing slight excess amounts of $GdCl_3.6H_2O$ salts and ligands in aqueous solution at pH 6.0 and purified by reverse phase column chromatography. Finally, we investigated the conversion of gadolinium complex **Gd-OH** into the corresponding triethoxysilane derivative **Gd-Si(OEt)$_3$**.

The preparation of **Gd-Si(OEt)$_3$** was achieved by the reaction of hydroxyl function of **Gd-OH** and the isocyanate function of the heterobifunctional reagent TESPIC, capable of two distinct sequential reactions.

*Surface functionalization of **NPSiO$_2$-NH$_2$** with **Gd-COOH** : **NPSiO$_2$-NHCO-Gd***

NH_2-functionalized silica NPs have been prepared according to already described procedures.[24] Their average size was determined by TEM (Figure ESI 3) and DLS (24.6 ± 2.7 nm and 196 nm ± 24% respectively), and the surface density of reactive NH_2 functional groups was estimated at 0.5 N/nm² on the basis of fluorescamine titration (see ESI). The **Gd-COOH** complex was reacted overnight with a dispersion of these NPs in PBS (10mM, pH= 7.4) at r.t. using EDC and sulfo-NHS as coupling agents.

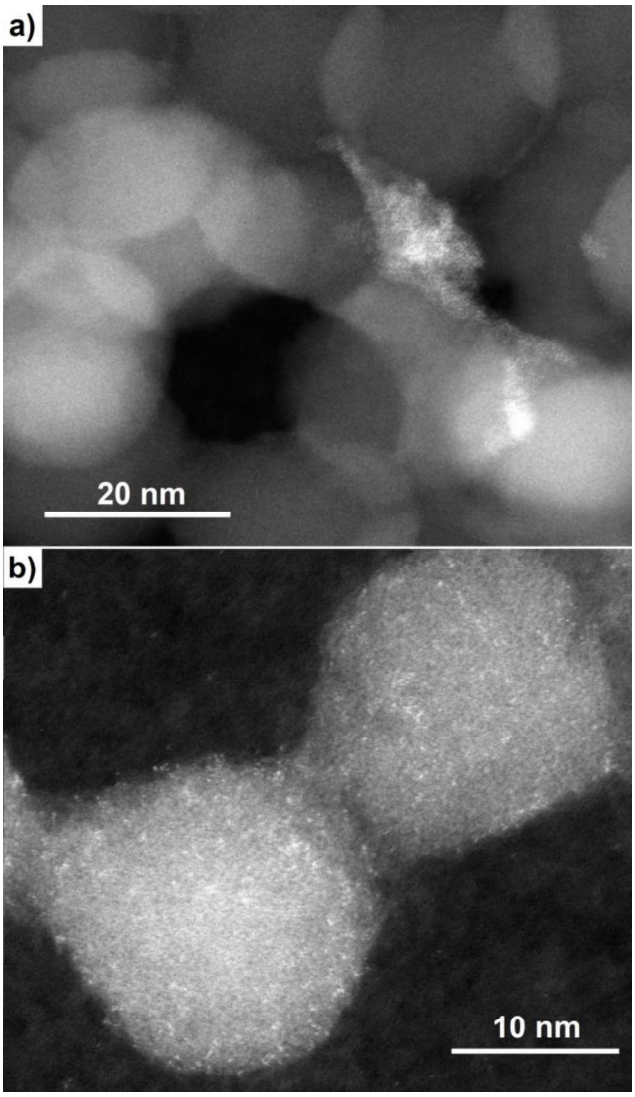

Figure 4. top : ARM image of **NPSiO$_2$-NHCO-Gd** showing a brighter area enriched in Gd according to EDX analysis (Figure ESI 12); bottom: ARM image of **NPSiO$_2$-Gd** showing the homogeneous distribution of Gd atoms onto the silica NPs.

After purification, the nanoparticles were not stable in solution. This prevented the determination of their hydrodynamic size by DLS analysis. ICP analysis confirmed the

incorporation of Gd in the nanomaterial up to 0.35 w% which would correspond to a grafting density of 0.1 Gd/nm². The IR spectrum of the powder (Figure ESI 10) displayed peaks of very weak intensity at 2981 and 2917cm^{-1} corresponding to the propyl chain of the surface functional groups and a peak of weak intensity at 1740 cm^{-1} which was tentatively attributed to an amide function confirming the presence of the Gd complex. TEM analysis of a dispersion of the NPs evidenced NPs of 25.9 ± 3.8 nm in diameter (Figure ESI 11). ARM analyses with a STEM-HAADF probe showed mostly NPs with non-evenly distributed brighter spots (Figure 4, top). EDX analysis confirmed that Gd was preferentially located in these regions (Figure ESI 12). Several attempts to graft the **Gd-COOH** complex have been undertaken, but the results were not reproducible and the process couldn't be optimized to get a homogeneous distribution of the complexes on the surface of the $NPSiO_2$. Variation of the reactant concentrations and ratios and of the reaction temperature didn't lead to any improvement. In a control experiment the **Gd-COOH** complex was mixed with the **$NPSiO_2$-NH_2** solution and stirred 65h at r.t.. After purification the nanomaterial contained the same weight percentage of Gd.

*Surface functionalization of **$NPSiO_2$** with **Gd-Si(OEt)$_3$** : **$NPSiO_2$-Gd***

The silica NPs were prepared following the protocol established in our group.[23] Their average size was determined by TEM (Figure ESI 2) and DLS (23.1 ± 3.6 nm and 104 nm ± 16 % respectively). The IR spectrum of the **$NPSiO_2$** was recorded in DRIFT mode to increase the signal over noise ratio (Figure ESI 14). It displayed mainly a large peak around 1093 cm^{-1} attributed to Si-O vibration bands, and an absorption at 1650 cm^{-1} indicative, with the large hump above 3000 cm^{-1}, of the presence of adsorbed water. The weak signal at *circa* 2960 cm^{-1} could be attributed to ν(C-H) vibrations of the ethoxy groups.

Grafting of the **Gd-Si(OEt)$_3$** complex on **$NPSiO_2$** was achieved after 48h in a 2/1 (v/v) water/ethanol mixture. Hydrolysis of the ethoxysilane groups onto the silica was catalyzed by ammonia. After purification, the functionalized NPs were suspended in milliQ water and this solution was analyzed by DLS, TEM and ICP-OES. An aliquot was lyophilized to yield a white powder, which was analyzed by DRIFT (Figure ESI 14) and gave a first indication of the presence of the Gd complex in the nanomaterial: signals at *circa* 2850-2930 cm^{-1} were attributed to the ν(C-H) stretching vibrations of the aliphatic chain of the Gd complex; peaks characteristic of the PCTA backbone were also observed in the 1400 – 1460 cm^{-1} region (see the IR spectra in ATR mode of **Gd-OH** and **Gd-Si(OEt)$_3$** in Figure ESI 13). However the signatures of the urethane and carboxylate functions couldn't be observed due to the relatively large contribution of adsorbed water close to 1650 cm^{-1}. A careful analysis of the TEM images (Figures ESI 2 and ESI 15) indicated no significant change in the average diameter of the NPs (23.1 ± 3.6 nm and 22.5 ± 3.5 nm for **$NPSiO_2$** and **$NPSiO_2$-Gd** respectively). Observation of the sample in high resolution in STEM-HAADF mode, showed bright dots corresponding to heavy atoms regularly dispersed at the surface of the NPs (Figure 4, bottom). EDX analysis of a concentrated region confirmed that these dots corresponded to Gd (Figure ESI 16). ICP-OES analysis allowed estimating the grafting density: 0.6 Gd/nm². This indicated that only one tenth of the complexes engaged in the reaction were successfully grafted. DLS analysis of the solution showed a slight increase of the hydrodynamic diameter from 104 nm (**$NPSiO_2$**) to 138 nm (**$NPSiO_2$-Gd**) as reported in Table 1

but the zeta potential was in both cases below -30mV for pH>5, in agreement with the low density of grafted complexes. Still, the isoelectric pH value increased from 2 to 3.5 upon grafting of the Gd complex, in agreement with a reduction of the number of accessible silicate ($Si\text{-}O^-$) groups at the surface of the NPs. These results were reproducibly obtained indicating the robustness of the synthetic procedure.

The same procedure was repeated to graft PEG chains at the surface of the **$NPSiO_2$-Gd** sample to get dispersions with increased stability and potentially better biocompatibility. Moreover, increasing the steric hindrance around the Gd complexes could limit their τ_R thus favouring their efficiency in MRI. The DRIFT spectrum of the final material (Figure ESI 14) showed a slight modification of the CH vibration bands in the 3000-2800 cm^{-1} region in agreement with the presence of the PEG chain. This nanomaterial presented similar hydrodynamic size (Table 1), zetapotential (below -30mV for pH>5) and isoelectric pH (3.5) to the **$NPSiO_2$-Gd** sample which was related to the low density of PEG chains grafted (< 0.03 PEG/nm^2 based on CHN analysis). Interestingly, no reduction of the Gd content could be detected by ICP-OES indicating a good stability of the SiO_2-Gd linkage.

Table 1 : Z-Average hydrodynamic diameters of **$NPSiO_2$**, **$NPSiO_2$-Gd**, **$NPSiO_2$-Gd-PEG, $NPSiO_2$-NH_2** and **$NPSiO_2$-NHCO-Gd** in milliQ water.

Sample	***$NPSiO_2$***	***$NPSiO_2$-Gd***	***$NPSiO_2$-Gd-PEG***	***$NPSiO_2$-NH_2***	***$NPSiO_2$-NHCO–Gd***
Z-Average diameter	104	138	140	196	Not measurable
PDI	15%	16%	19%	24%	/
ZP (mV) at pH = 7	-33	-33	-38	-35	/
pHi	2.5	3.3	3	5.7	/

Relaxivity assessments

Study of the free complexes

The NMRD profiles of the three Gd-PCTA complexes prepared (**Gd-COOH**, **Gd-OH** and **Gd-Si(OEt)$_3$**) were recorded at 37°C (see Figure 5). Their shape was typical of the one displayed by molecular gadolinium complexes in solution with plateaus at low and then moderate fields followed by a further decrease of the relaxivity at high field.[2] The fitting of the data was performed according to the SBM model,[27–29] assuming that the contribution of the outer-sphere mechanism was comparable for the three complexes, and that the water–Gd distance was the same in each case, as the modification of the complex involved only a change in the pendant group of the ligand. It allowed us to estimate the τ_R of the complexes (see Table 2). The τ_R values obtained for the complexes with pendant hydroxy and carboxylic functions were both close to *circa* 80ps*, i.e.* very close to the one reported for the parent non-functionalized PCTA-Gd complex (*circa* 70ps[34]). But the τ_R of the silylated complex **Gd-Si(OEt)$_3$** was twice higher.

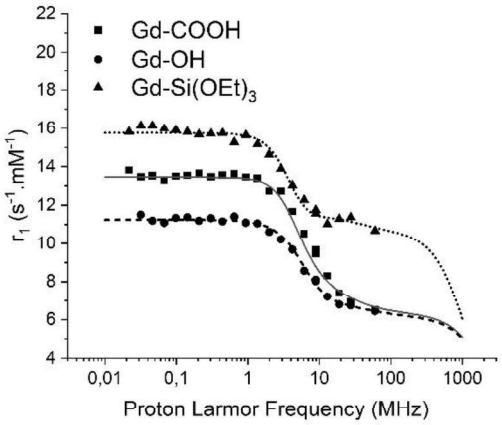

Figure 5 : NMRD profiles of **Gd-COOH** (2.6 mM, full squares), **Gd-OH** (3.7 mM, full circles), and **Gd-Si(OEt)$_3$** (3 mM, full triangles) complexes (T=37°C) and their corresponding fits (respectively solid, dashed and dotted lines).

Table 2 : Physicochemical data obtained from the fitting of the NMRD profiles (values fixed for the fitting: d=0.36 nm ; D= 3.3 10^{-9} m².s^{-1}; r=0.31 nm; q=2, τ_M = 100ns). τ_R: rotational correlation time, τ_{SO}: electronic relaxation time at very low fields ; τ_V: correlation time describing the modulation of the zero field splitting.

	Gd-COOH	***Gd-OH***	***Gd-Si(OEt)$_3$***	***NPSiO$_2$-Gd***	***NPSiO$_2$-Gd-PEG***
τ_R	80.6 ± 1.8 ps	78.2 ± 1.8 ps	151 ± 2 ps	2.1 ± 0,001 ns	3.06 ± 0.002 ns
τ_{S0}	131 ± 2 ps	83.5 ± 2.1 ps	106 ± 2 ps	358 ± 2 ps	857 ± 2 ps
τ_V	41.3 ± 1.6 ps	20.5 ± 1.6 ps	40.5 ± 2.2 ps	35.0 ± 1.6 ns	30.0 ± 1.6 ps

Their longitudinal and transversal relaxivities (r_1 and r_2) as well as those of DOTAREM® were measured at 37°C at 20MHz (0.47 T) and 60 MHz (1.5 T). The results are reported in Table 3. **Gd-COOH** and **Gd-OH** complexes displayed quasi identical relaxivities that were significantly higher than those of the reference CA in agreement with the difference in coordinated water molecules. Their longitudinal relaxivity values at 60MHz were also slightly higher than the one reported in the literature[35] for the parent non-functionalized Gd-PCTA complex (r_1 = 5.9 s^{-1}.mM^{-1}) in agreement with their higher τ_R (78.2 ps for Gd-OH ; 70 ps for Gd-PCTA).[34]

As can be seen in Table 3, the **Gd-Si(OEt)$_3$** complex displayed an even higher longitudinal relaxivity (r_1 (20MHz) = 9.7 s^{-1}.mM^{-1} ; r_1 (60MHz)= 10.65 s^{-1}.mM^{-1}) as expected from the study of its NMRD profile. In all cases the r_2/r_1 ratio was close to 1, the expected value for a valuable CA in T_1-weighted MRI.

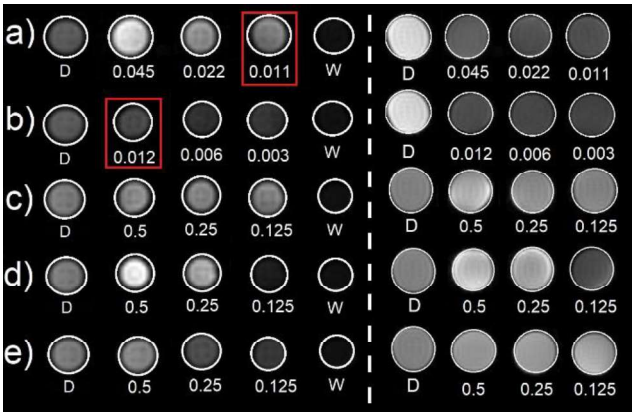

Figure 6 : T_1-weighted MRI images recorded on phantoms at 1T(40MHz) (left) and 9.4T(400MHz) (right) of a) **$NPSiO_2$-Gd**, b) **$NPSiO_2$-Gd-PEG** c) **Gd-OH**, d) **Gd-Si(OEt)$_3$** and e) **Gd-COOH**. Concentrations are given in Gd [mM], D = DOTAREM® at 0.5 mM and W = water.

T_1-weighted MRI images were recorded on phantoms at 1T over a 0.125-0.5mM concentration range (Figure 6). The contrast induced on the images by the Gd-OH complex was higher than the contrast produced by the same concentration of DOTAREM®, and the contrast induced by the **Gd-Si(OEt)$_3$** complex was much higher as expected from the relaxivity values at 20 and 60 MHz. At 9.4 T, **Gd-OH** and **Gd-Si(OEt)$_3$** complexes were also more efficient than DOTAREM®, with a more pronounced contrast in the case of the silylated complex.

Such complexes could thus be of interest as CA in high field MRI, contrarily to DOTAREM®, at least in pre-clinical studies.[12]

Table 3 : Relaxivity values at 37°C. Values at 400MHz were deduced from the contrast observed in the phantom images. CA1: DTPA-Gd complex supported on MCM-48 NPs;[36] CA2: DOTAGA-Gd complex supported on home-made mesoporous silica NPs;[37] CA3: DTPA-Gd complex supported on MCM-48 NPs.[38]

Frequency (MHz)	*Relaxivity ($s^{-1}.mM^{-1}$)*	*DOTAREM®*	***Gd-COOH***	***Gd-OH***	***Gd-(SiOEt)$_3$***	***$NPSiO_2$-Gd***	***$NPSiO_2$-Gd-PEG***	*CA1[36]*	*CA2[37]*	*CA3[38]*
20 MHz (0.47 T)	r_1	4.1	7.97	7.65	9.7	62	80	≅22	79.1	/
	r_2	4.9	9.27	9.14	11.8	77	119	≅27	/	/
	r_2/r_1	1.2	1.16	1.19	1.2	1.22	1.48	1.2	/	/
60 MHz (1.5 T)	r_1	3.7	6.93	6.75	10.65	56	65	17.6	≅48	23.97
	r_2	4.0	8.12	7.82	12.3	104	148	35.3	/	35.33
	r_2/r_1	1.08	1.17	1.16	1.17	1.8	2.27	2	/	1.47
400 MHz (9.4 T)	r_1	4.67	9.6	10.3	18.9	75	83	/	/	/

Study of the immobilized complexes

The same study was carried out once the complexes were grafted onto silica NPs, before and after pegylation of the surface *i.e.* on samples **NPSiO$_2$-Gd** and **NPSiO$_2$-Gd-PEG**. The corresponding NMRD profiles, as well as the best fit obtained, are given in Figure 7 and the parameters extracted from the fitting procedure are reported in Table 2.

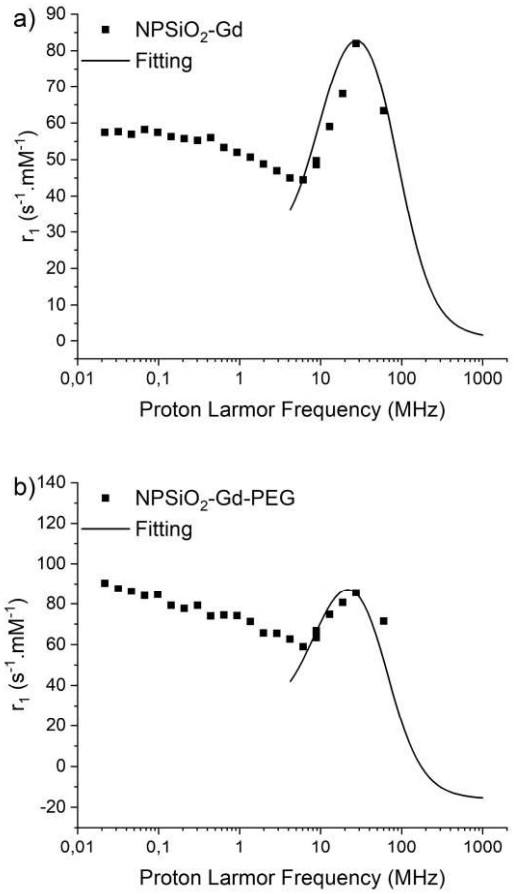

Figure 7. NMRD profiles at T=37°C of a) **NPSiO$_2$-Gd** at 60 µM of Gd and b) **NPSiO$_2$-Gd-PEG** at 12 µM of Gd. Data corrected from the contribution of silica.

The NMRD profiles are typical of Gd chelates « grafted » or « coordinated » to larger entities such as peptides or nanoparticles,[39] with a slow decrease until 10 MHz followed by a rise towards a maximum around 60 MHz and a large drop at high field. Also the τ_R reached 2-3 ns, values very close to those reported by Carniato *et al.*[15] for Gd-DOTAGA complexes immobilized on mesoporous silica NPs. Accordingly, a drastic increase of the r_1 value (from 9.5 $s^{-1}.mM^{-1}$ for the free complex to 62-68 $s^{-1}.mM^{-1}$ once grafted) was observed at 20MHz. A similar variation was observed at 60MHz.

A clear increase of their transversal relaxivity r_2 was also observed once the complexes were grafted on the silica NPs. But the r_2/r_1 ratios remained close enough to 1 for the **NPSiO$_2$-Gd** and **NPSiO$_2$-Gd-PEG** samples, suggesting that these nanomaterials would give a good contrast in T_1-weighted MRI images.

The T_1-weighted MRI images of phantoms recorded at 1T (40 MHz) and 9.4T (400 MHz) confirmed this interpretation. Indeed, at 10 times lower concentrations, the contrast

provided by **$NPSiO_2$-Gd** at 1T was already much stronger than the one induced by DOTAREM®. Comparison between the phantoms of the **$NPSiO_2$-Gd** before and after pegylation (highlighted by squares on Figure 6), showed that the pegylated system was a little less efficient. Nevertheless it provided a much better contrast than DOTAREM®. At 9.4T, the contrast induced by these nanomaterials was weaker as expected from their NMRD profiles.

Cytotoxicity assessments

Cytotoxicity assays were performed using a human colon cancer cell line, HCT116, and a non-tumoral fibroblast cell line: 1BR3G (transformed human skin fibroblasts).

We first tested the Gd complexes as only limited data are reported in the literature on PCTA-Gd complexes. **Gd-Si$(OEt)_3$** solutions were not stable enough in the conditions required for these assays and its cytotoxicity could not be evaluated. **Gd-COOH** and **Gd-OH** complexes have been studied at concentrations up to 1mM (see Figure 8 and Figure 9). All the results were reproducibly observed.

The **Gd-COOH** complex was better tolerated by the HCT116 cells than the **Gd-OH** one, with cell viability dropping below 80% only for concentrations above 0.7mM after 72h of incubation, while **Gd-OH** complex already displayed a significant drop in cell viability after 24h of incubation at 0.2mM. The median inhibitory concentration (IC_{50}) of this complex on HCT 116 cells was roughly estimated at 0.5 mM (72h of incubation). The same trend was observed on 1BR3G cells but at somewhat higher concentrations: IC_{50} closer to 0.7mM for the **Gd-OH** complex after 72h of incubation, while cell viability remained above 80% for the **Gd-COOH** complex in these conditions.

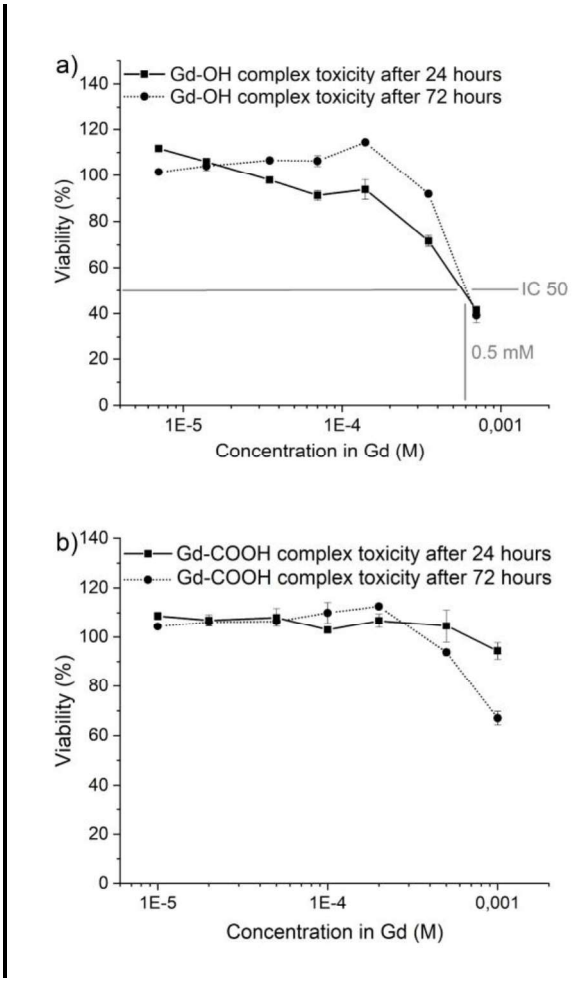

Figure 8 : Cell viability (HCT116 cell line) as a function of the Gd concentration after 24 and 72h of incubation at 37°C with a) **Gd-OH** and b) **Gd-COOH**.

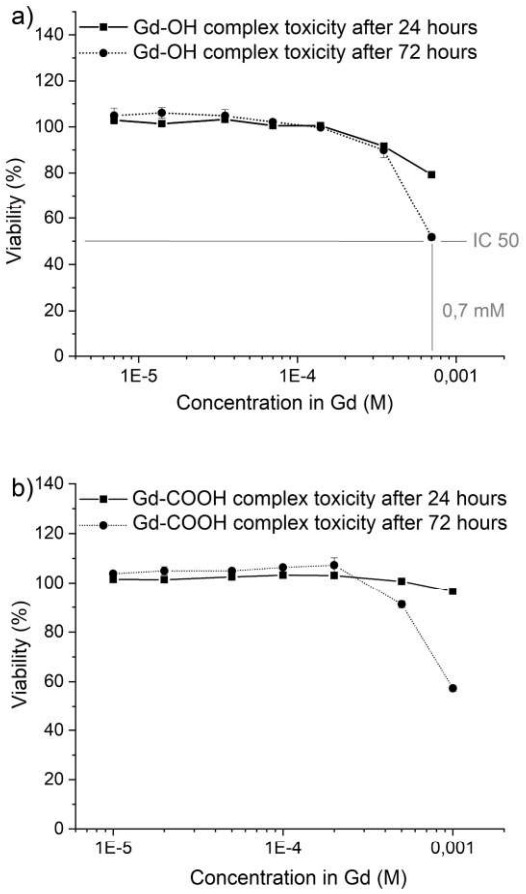

Figure 9 : Cell viability (1BR3G cell line) as a function of the Gd concentration after 24 and 72h of incubation at 37°C with a) **Gd-OH** and b) **Gd-COOH**.

The functionalized **$NPSiO_2$** (**$NPSiO_2$-Gd** and **$NPSiO_2$-Gd-PEG** samples) were tested against the same cell lines by working with a maximum concentration of 200 μg.mL^{-1} of NPs *i.e.* [Gd] ≅ 0.08 mM to ensure that no precipitation occurred during the experiments. Comparison was made with pure silica NPs synthesized according to the same procedure ($NPSiO_2$ as described in ESI, Figure ESI2) in order to try and evidence any possible adverse effect of gadolinium. All the results were reproducibly observed.

Cell viability (reported on Figure 10) in the presence of the NPs at [NPs] of 100 μg/mL (*i.e.* [Gd] ≅ 0.04 mM) was above 90% whatever their surface state (with or without Gd(III) complex, with and without pegylation) even after 72h of incubation with the highest concentration studied (200μg.mL^{-1} *i.e.* [Gd] ≅ 80 μM) see Figure ESI 17.

The concentration range studied wasn't large enough to determine the IC_{50} for these nanomaterials, but was centred on the values which would be used to get a good MRI signal over noise ratio.

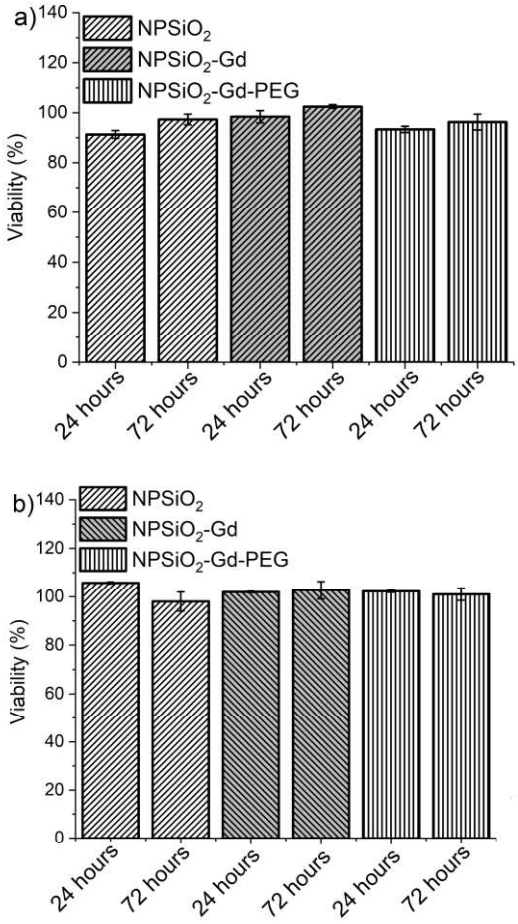

Figure 10 : Viability of a) HCT 116 and b) 1BR3G cell lines, after 24 and 72 h of incubation at 37°C in the presence of NPs (100 $\mu g_{NPs}.mL^{-1}$ *i.e.* [Gd] ≅ 0.04 mM).

Discussion

Synthesis

Nanomaterials are often used to locally concentrate Gd complexes and at the same time form a paramagnetic nanomaterial with limited rotation and diffusion motions due to its elevated molecular weight and large hydrodynamic radius. Here we chose to use dense amorphous silica NPs to support Gd complexes for many reasons. Amorphous silica NPs is a low cost, non-toxic material already used as food additives and extensively studied in biomedical applications such as drug delivery.[40–42] It dissolves into the non-toxic silicic acid in the body, and this substance can be filtrated by the kidneys and removed from the blood through urine.[43–46] The silica NPs used in this work were easily grown following the well-known Stöber process in reverse micelles that leads to an amorphous material.[23] If needed, the NPs size can be easily adjusted and their surface chemistry is well known. Then, it was demonstrated previously that mesoporous silica NPs, if interesting for drug delivery, were not so interesting to develop diagnostic contrast agents as diffusion of water inside the mesopores is very slow and consequently only the complexes grafted at the external surface of these NPs could effectively increase the relaxivity of the water molecules.[37] This

reinforced us in the use of dense amorphous silica NPs as a support. Still to reduce the molecular tumbling rate of the Gd complexes, once grafted on the $NPSiO_2$, we decided to graft the complexes via a relatively short anchoring chain (of 7 to 13 atoms). And further, we grafted PEG chains in the space left available at the surface of the silica NPs, keeping a low grafting density not to limit the access of water to the coordination sphere of the Gd ions. Moreover, PEG coatings generally increase the stability of colloidal solutions at physiological pH, and the biocompatibility and blood circulation half-life time of the NPs, which is especially important for CA destined to image tumors.[16]

We chose to use PCTA modified ligands to chelate Gd(III) ions because the PCTA-Gd complexes offer the best compromise between large hydration number, good *in vivo* stability and high kinetic inertness, and short residence lifetime of the water molecules in the coordination sphere of Gd(III).[11]

Two routes can be followed to produce immobilized Gd complexes on silica NPs : i) grafting of the ligand, then complexation of the Gd(III) ion on the immobilized ligand or ii) formation of the Gd complex before grafting it on the silica surface. The first route might lead to unspecific adsorption of free Gd(III) ions or Gd hydroxydes at the surface of silica affording nanomaterials with possible traces of these toxic ions which are particularly difficult to eliminate.[15] So the second route has been chosen in this work. Two main strategies are usually followed to attach molecular species onto silica surfaces and particularly to develop efficient CAs[47,48] : i) amidic coupling and ii) condensation of alkoxysilanes. To test these approaches we designed modified PCTA ligands presenting either $-Si(OEt)_3$ or -COOH pendant functional groups to be anchored on silica nanoparticles, naked or previously modified with APTMS to expose NH_2 functionalities. The corresponding Gd complexes as well as the parent PCTA complex and the most currently used MRI contrast agent DOTAREM® are presented in Figure 1; and immobilization pathways are presented in Figure 2.

The synthetic methodology for accessing PCTA derivatives, developed by some of us, was convenient to prepare two new PCTA chelators bearing a carboxylic acid or triethoxysilane function available for grafting chelates on silica NPs. These reactive groups were introduced on the 4-position of the pyridine ring in order to limit any interference with the ion coordination sphere in the corresponding Gd(III) complexes. In this direction, we can notice that the introduction of a linker on the 3-position of the PCTA pyridine ring can lead to a decrease in the number of coordinated water molecules in Gd(III) complexes, and therefore lower the relaxivity of complexes.[11] In the synthesis of these bifunctional ligands, we have observed again the presence of an efficient sodium template effect for the crucial macrocyclization step. As expected, the different ^1H NMR signatures of Na^+-adduct and Na^+-free forms avoid mistakes about the characterization of purified materials. For example, ^1H and ^{13}C NMR data of Na^+-adduct and Na^+-free forms of **9** are gathered in the experimental part.

Amidic coupling (Figure 2, left pathway)was carried out in water to make sure no potentially toxic solvent (such as *e.g.* CH_2Cl_2, DMSO or DMF) would remain adsorbed on the silica NPs afterwards. We used the EDC/sulfoNHS couple to trigger the reaction as this is the most

popular type of zero-length crosslinker used in water to immobilize *e.g.* proteins on amine terminated beads of various sorts.[49] We used fluorescamine to quantify the number of available NH_2 functions prior to carrying out the amidic coupling reaction. Indeed, the aminopropyl chain can bind on itself and interact with the silica surface, and/or some of the NH_2 functions can be trapped during the condensation of APTMS at the surface of the silica NPs during the first functionalization step (see Figure 2, left pathway) thus decreasing the number of available NH_2 functions.. As expected this number was lower than the number of NH_2 groups determined on the basis of CHN analysis (0.5 and 2 NH_2/nm^2 respectively) but consistent with previously reported results[26,50] and clearly confirmed the presence of reactive NH_2 functions. However in our hands, despite many trials, the amidic coupling only conducted to poor results. Only a very limited quantity of Gd could be detected in the final nanomaterial. As aggregates of Gd complexes were observed at the surface of the nanomaterial, the poor success of the reaction was first attributed to a partial aggregation of the **$NPSiO_2$-NH_2** in solution. Moreover, control experiments carried out in the absence of coupling agent gave similar results suggesting that the interaction observed was mainly non-specific. It could result from a simple mechanical trapping at necks between aggregated **$NPSiO_2$-NH_2**. Grafting PEG chains at the surface of the NPs might have imparted a better stability to the colloidal solution of **$NPSiO_2$-NH_2**, however it would also have increased steric hindrance and disfavoured the coupling of the **Gd-COOH** complex with the NH_2 surface functions.[38] We didn't push any further our investigations on this system.

Condensation of the **Gd-Si(OEt)$_3$** complex on **$NPSiO_2$** (Figure 2, right pathway), lead to highly reproducible results with a regular distribution of the Gd complexes at the surface of the NPs and surface coverage of 0.6 Gd/nm^2 close to the one obtained by Cheng *et al.*[51] when immobilizing Si-DTTA-Gd complexes on dense silica NPs via a siloxane linkage (≅1Gd/nm^2). From the zetapotential of the NPs (-33mV at pH=7), it can be deduced that a significant quantity of silanol surface groups (deprotonated) is still available and can be used to give another functionality to the nanosystem (biocompatibility, vectorisation, therapeutics ...) which we have illustrated in grafting PEG chains.

Relaxometry

The relaxivity values (r_1 and r_2) of the **Gd-COOH** and **Gd-OH** complexes measured at 20 and 60MHz (37°C) were larger than those measured for DOTAREM® (see Table 3) in agreement with the higher number of water molecules in the coordination sphere of the paramagnetic Gd(III) ion and higher rotational correlation times. They were also larger than reported for the parent Gd-PCTA complex (r_1 = 5.9 $s^{-1}.mM^{-1}$, 60MHz)[35] which could be related to their slightly larger rotational correlation times. Surprisingly, the τ_R of the silylated complex **Gd-Si(OEt)$_3$** was twice higher. In a first approach, this was related to its higher molecular weight or to a beginning of condensation of this complex on itself due to a slow hydrolysis of the ethoxysilane functions, here again affording clusters of high molecular weight and restricted tumbling, the τ_R of which would necessarily be higher. Accordingly, as can be seen in Table 3, this complex displayed a high longitudinal relaxivity value (r_1 (20MHz) = 9.7 $s^{-1}.mM^{-1}$; r_1 (60MHz) = 10.65 $s^{-1}.mM^{-1}$). In all cases, it is noteworthy that the r_2/r_1 ratio was close to 1, the expected value for a valuable CA in T_1-weighted MRI. This was confirmed by the good contrast observed in T_1-weighted MRI images recorded at 1T (37°C). Indeed, the complexes

described herein displayed superior efficiency as compared to DOTAREM®. Interestingly the **Gd-OH** and **Gd-Si(OEt)$_3$** complexes induced also a much better contrast than DOTAREM® at 9.4T (37°C). These complexes could thus be of interest as CAs in high field MRI contrarily to DOTAREM®, enabling higher resolution images with shorter acquisition times, at least in pre-clinical studies.

The immobilized complexes displayed enhanced relaxivity values at 20 and 60MHz as compared to the free complexes which confirmed that their tumbling was considerably slowed down upon conjugation at the surface of the silica NPs. Fitting of their NMRD profiles indeed indicated τ_R values in the 2-3ns range. While both their longitudinal as well as transversal relaxivity increased, their ratio remained close to the optimum value for a T_1-weighted CA. Once again, the contrast observed on T_1-weighted images of phantoms recorded at 1T confirmed this first analysis. For instance, the contrast induced at 1T (37°C) by the **NPSiO$_2$-Gd** or **NPSiO$_2$-Gd-PEG** systems was better than the one provided by DOTAREM® even at 10 times lower concentrations in Gd.

Although the grafting of Gd complexes on silica has already been reported by many authors, few measurements were carried out in conditions comparable to ours (in terms of field and temperature).[52] For example, immobilization of DOTAGA-Gd complexes on mesoporous silica NPs lead to r_1 values as high as 79.1 $mM^{-1}.s^{-1}$ at 20 MHz but fast decreasing at 60 MHz (≅48 $mM^{-1}.s^{-1}$).[37] Gd-DTPA-Si complexes immobilized on MCM-48 NPs displayed r_1 values in the range 17 to 24 $mM^{-1}.s^{-1}$ and r_2 values close to 35$mM^{-1}.s^{-1}$[136,38] at 60MHz (*i.e.* r_2/r_1 ratios varying from 1.47[38] to 2[36] at 60MHz, see Table 3 for values at 20MHz). In comparison, the CA reported here give larger r_1 values especially at 60 MHz (1.5T), the most commonly used field in clinical MRI and the r_2/r_1 ratio stays very low (<2.3), close to the optimal value expected for a T_1-weighted MRI contrast agent. The very good results obtained in this work show that the modified PCTA-Gd complexes immobilized on the silica NPs remained readily accessible to the water molecules rather than being partially embedded in a siloxane surface layer,[51,53] or trapped inside pores[54] contrarily to what is sometimes observed in sol-gel chemistry and was observed here when grafting APTMS molecules on $NPSiO_2$. This, combined with the large τ_R obtained, validates the choice of the linker and method used to immobilize the Gd-PCTA complex (**Gd-Si(OEt)$_3$**) on the silica NPs.

Cytotoxicity

Gd-OH complex displayed more toxicity towards the cells than the **Gd-COOH** one. The difference in cytotoxicity was directly related to the different functional groups present on the pyridinic carbon of the PCTA backbone of the complex. Indeed at the pH of the incubation medium, the complex was present in its deprotonated form, hence displayed a negative charge which would less interact with the cells membrane in comparison with the neutral **Gd-OH** complex. Still the IC_{50} after 72h of incubation was above the concentration of interest for MRI usage (*e.g.* DOTAREM® preparations have a concentration of 0.5mM in Gd). In the case of the immobilized complex, **NPSiO$_2$-Gd** and **NPSiO$_2$-Gd-PEG** samples, the stock solution prepared for the cytotoxicity evaluation (200µg.mL^{-1} of NPs) displayed a Gd concentration of [Gd]≅ 0.08 mM which is almost twice the concentration used in the phantom displaying the brightest image obtained at 1T in T_1-weighted MRI images (Figure 6).

Even in these conditions, 90 to 100% cell viability was observed depending on the cell lines (Figure ESI 17), like for **$NPSiO_2$** sample studied in a control experiment. It clearly shows that immobilization of the complexes onto the silica surface provided a non-toxic CA with improved relaxivity and contrast enhancement in MRI images, at least towards the two cell lines tested (one cancerous and one normal).

Conclusions

The synthesis of highly effective T_1 contrast agents has been achieved thanks to the design of functional bis-hydrated Gd-PCTA complexes and their grafting on the surface of dense silica nanoparticles. Among the two synthetic pathways investigated (amidic coupling and alkoxysilane condensation), condensation of a triethoxysilane derivative of the PCTA complex gave the most homogeneous and reproducible nanomaterial. Complete characterization of the complexes before and after immobilization on the silica NPs has been achieved by the use of complementary techniques. Their efficiency as T_1 contrast agents and their cytotoxicity on two different human cell lines (normal and cancerous) have been evaluated. The nanomaterials displayed a very good colloidal stability in a wide pH range (ζ = -30 mV from pH = 5 to pH = 10) with hydrodynamic diameters around 140nm, and no toxicity after 72 hours of incubation with 1BR3G and HCT116 cells around the concentration of interest for MRI. The relaxometry analysis and MRI images (recorded on phantoms) showed that the Gd-PCTA complexes induce an improved contrast compared to the DOTAREM® which can be directly attributed to the number of water molecules in the coordination sphere (q=2). Grafting of this complex on the silica nanoparticles increased even more the relaxivity values of the gadolinium. Fitting of NMRD profiles evidenced the increase in τ_R in agreement with the increased r_1 values, as expected by the large hydrodynamic diameter and weight of the nanohybrid formed. Imaging of phantoms suggested that the concentration of Gd to be injected could be decreased by a factor of 10 while still providing a good contrast in the images. Yet, more data need to be acquired, this time *in vivo* to confirm these promising results. The silica support used in this work offers multiple advantages, like multistep functionalisation which was simply illustrated here by post-grafting PEG chains on the **$NPSiO_2$-Gd** contrast agent. This post-grafting step didn't induce any significant change of the imaging properties and cytotoxicity results. One could thus take advantage of this surface reactivity to anchor molecular targeting vectors to convey the CA to the organ under study to further limit the dose to be injected to the patients and also to facilitate the reading of the images. It is also of interest in order to tune the pharmacokinetics of the CA, which toxicity *in vivo* also depends on.[48] Finally the core of these silica NPs can also be tuned. For example, we previously synthesized and reported a nano-contrast agent composed of iron/iron oxide nanoparticles coated with silica,[23] which displayed high r_2 relaxivity, and efficient contrast in T_2–weighted MRI images as well as low cytotoxicity. Grafting of the Gd complexes reported herein onto NPFe@FeOx@SiO_2 is currently under investigation to afford a bimodal T_1/T_2 contrast agent which should allow a better interpretation of the MRI images by ruling out false positive as well as false negative results.[55]

Supporting information: list of abbreviations; protocols and TEM analysis for pure silica NPs (**$NPSiO_2$**) and NH_2 modified silica NPs (**$NPSiO_2$-NH_2**); ^1H and ^{13}C NMR spectra of compounds **10** and **12** ; mass spectra of **Gd-COOH** and of **Gd-OH** complexes ; complementary data on the

amidic coupling between **$NPSiO_2$** and **Gd-COOH** (IR spectra, TEM and EDX analysis), on the condensation between **$NPSiO_2$** and **Gd-$Si(OEt)_3$** (IR spectra, TEM and EDX analysis) and on the cytotoxicity evaluation.

Funding: This research was funded through the C-NIM project (ESR_R&S_DF-000003/2017-006704) and by the Spanish Ministry of Sciences, Innovation and Universities through the project RTI2018-098027-B-C22. The CMMI is supported by the European Regional Development Fund and the Walloon Region (Wallonia-Biomed portfolio, #411132-957270).

Acknowledgments: P.M. thanks University of Toulouse for his PhD grant. We thank Vincent Collière for his help in collecting the TEM data and Corinne Routaboul for her help in recording the IR spectra in DRIFT mode.

Conflicts of Interest: The authors declare no conflict of interest.

1 D. Ni, W. Bu, E. B. Ehlerding, W. Cai and J. Shi, *Chem. Soc. Rev.*, 2017, **46**, 7438–7468.
2 P. Caravan, *Chem. Soc. Rev.*, 2006, **35**, 512.
3 P. Caravan, C. T. Farrar, L. Frullano and R. Uppal, *Contrast Media Mol. Imaging*, 2009, **4**, 89–100.
4 Z. Zhou and Z.-R. Lu, *Wiley Interdiscip. Rev. Nanomed. Nanobiotechnol.*, 2013, **5**, 1–18.
5 J. Wahsner, E. M. Gale, A. Rodríguez-Rodríguez and P. Caravan, *Chem. Rev.*, 2019, **119**, 957–1057.
6 S. Laurent, C. Henoumont, D. Stanicki, S. Boutry, E. Lipani, S. Belaid, R. N. Muller and L. Vander Elst, *MRI Contrast Agents: From Molecules to Particles*, Springer Singapore, Singapore, 2017.
7 P. Caravan, J. J. Ellison, T. J. McMurry and R. B. Lauffer, *Chem. Rev.*, 1999, **99**, 2293–2352.
8 R. van Eldik, Ed., *Relaxometry of water-metal ion interactions*, Elsevier Acad. Press, Amsterdam, 2005.
9 M. Moula Karimdjy, G. Tallec, P. H. Fries, D. Imbert and M. Mazzanti, *Chem. Commun.*, 2015, **51**, 6836–6838.
10 L. Moriggi, C. Cannizzo, C. Prestinari, F. Berrière and L. Helm, *Inorg. Chem.*, 2008, **47**, 8357–8366.
11 M. Devreux, C. Henoumont, F. Dioury, D. Stanicki, S. Boutry, L. Larbanoix, C. Ferroud, R. N. Muller and S. Laurent, *Eur. J. Inorg. Chem.*, 2019, **2019**, 3354–3365.
12 P. Fries, J. N. Morelli, F. Lux, O. Tillement, G. Schneider and A. Buecker, *Wiley Interdiscip. Rev. Nanomed. Nanobiotechnol.*, 2014, **6**, 559–573.
13 W. Krause, Ed., *Magnetic resonance imaging*, Springer, Berlin, 2002.
14 Y.-F. Li and C. Chen, *Small*, 2011, **7**, 2965–2980.
15 F. Carniato, L. Tei and M. Botta, *Eur. J. Inorg. Chem.*, 2018, **2018**, 4936–4954.
16 F. Carniato, D. Alberti, A. Lapadula, J. Martinelli, C. Isidoro, S. Geninatti Crich and L. Tei, *J. Mater. Chem. B*, 2019, **7**, 3143–3152.
17 G. Tircsó, Z. Kovács and A. D. Sherry, *Inorg. Chem.*, 2006, **45**, 9269–9280.
18 R. Delgado, S. Quintino, M. Teixeira and A. Zhang, *J. Chem. Soc. Dalton Trans.*, 1997, 55–64.
19 G. Tircsó, E. T. Benyó, E. H. Suh, P. Jurek, G. E. Kiefer, A. D. Sherry and Z. Kovács, *Bioconjug. Chem.*, 2009, **20**, 565–575.
20 C. Galaup, J.-M. Couchet, S. Bedel, P. Tisnès and C. Picard, *J. Org. Chem.*, 2005, **70**, 2274–2284.
21 M. Enel, N. Leygue, N. Saffon, C. Galaup and C. Picard, *Eur. J. Org. Chem.*, 2018, **2018**, 1765–1773.
22 G. Zech and H. Kunz, *Chem. - Eur. J.*, 2004, **10**, 4136–4149.
23 P. Mathieu, Y. Coppel, M. Respaud, T. Q. Nguyen, S. Boutry, S. Laurent, D. Stanicki, C. Henoumont, F. Novio, J. Lorenzo, D. Montpeyó and C. Amiens, *Molecules*, 2019, **24**, 4629.
24 C. Tissandier, N. Diop, M. Martini, S. Roux, O. Tillement and T. Hamaide, *Langmuir*, 2012, **28**, 209–218.
25 Q. He, J. Zhang, J. Shi, Z. Zhu, L. Zhang, W. Bu, L. Guo and Y. Chen, *Biomaterials*, 2010, **31**, 1085–1092.
26 O. Makrygenni, E. Secret, A. Michel, D. Brouri, V. Dupuis, A. Proust, J.-M. Siaugue and R. Villanneau, *J. Colloid Interface Sci.*, 2018, **514**, 49–58.
27 I. Solomon, *Phys. Rev.*, 1955, **99**, 559–565.
28 N. Bloembergen, *J. Chem. Phys.*, 1957, **27**, 572–573.
29 N. Bloembergen and L. O. Morgan, *J. Chem. Phys.*, 1961, **34**, 842–850.
30 C. Henoumont, L. Vander Elst, S. Laurent and R. N. Muller, *J. Phys. Chem. B*, 2010, **114**, 3689–3697.
31 R. M. Supkowski and W. DeW. Horrocks, *Inorganica Chim. Acta*, 2002, **340**, 44–48.
32 M. Xu, D. J. McCanna and J. G. Sivak, *J. Pharmacol. Toxicol. Methods*, 2015, **71**, 1–7.
33 N. Leygue, M. Enel, A. Diallo, B. Mestre-Voegtlé, C. Galaup and C. Picard, *Eur. J. Org. Chem.*, 2019, **2019**, 2899–2913.
34 E. Brücher, G. Tircsó, Z. Baranyai, Z. Kovács and A. D. Sherry, in *The Chemistry of Contrast Agents in Medical Magnetic Resonance Imaging*, eds. A. Merbach, L. Helm and É. Tóth, John Wiley & Sons, Ltd, Chichester, UK, 2013, pp. 157–208.
35 S. Aime, M. Botta, S. G. Crich, G. Giovenzana, R. Pagliarin, M. Sisti and E. Terreno, *Magn. Reson. Chem.*, 1998, **36**, S200–S208.
36 M. Laprise-Pelletier, M. Bouchoucha, J. Lagueux, P. Chevallier, R. Lecomte, Y. Gossuin, F. Kleitz and M.-A. Fortin, *J. Mater. Chem. B*, 2015, **3**, 748–758.

37 F. Carniato, L. Tei, A. Arrais, L. Marchese and M. Botta, *Chem. - Eur. J.*, 2013, **19**, 1421–1428.
38 M. Bouchoucha, R. C.-Gaudreault, M.-A. Fortin and F. Kleitz, *Adv. Funct. Mater.*, 2014, **24**, 5911–5923.
39 R. B. Lauffer, *Chem. Rev.*, 1987, **87**, 901–927.
40 T. Asefa and Z. Tao, *Chem. Res. Toxicol.*, 2012, **25**, 2265–2284.
41 W.-T. Chan, C.-C. Liu, J.-S. Chiang Chiau, S.-T. Tsai, C.-K. Liang, M.-L. Cheng, H.-C. Lee, C.-Y. Yeung and S.-Y. Hou, *Int. J. Nanomedicine*, 2017, **Volume 12**, 3421–3432.
42 J. Lu, M. Liong, Z. Li, J. I. Zink and F. Tamanoi, *Small*, 2010, **6**, 1794–1805.
43 P. J. Kempen, S. Greasley, K. A. Parker, J. C. Campbell, H.-Y. Chang, J. R. Jones, R. Sinclair, S. S. Gambhir and J. V. Jokerst, *Theranostics*, 2015, **5**, 631–642.
44 J.-H. Park, L. Gu, G. von Maltzahn, E. Ruoslahti, S. N. Bhatia and M. J. Sailor, *Nat. Mater.*, 2009, **8**, 331–336.
45 T. Liu, L. Li, X. Teng, X. Huang, H. Liu, D. Chen, J. Ren, J. He and F. Tang, *Biomaterials*, 2011, **32**, 1657–1668.
46 S.-A. Yang, S. Choi, S. M. Jeon and J. Yu, *Sci. Rep.*, 2018, **8**. DOI:10.1038/s41598-017-18502-8.
47 C. Caltagirone, A. Bettoschi, A. Garau and R. Montis, *Chem. Soc. Rev.*, 2015, **44**, 4645–4671.
48 M. A. Bruckman, X. Yu and N. F. Steinmetz, *Nanotechnology*, 2013, **24**, 462001.
49 G. T. Hermanson, *Bioconjugate techniques*, Academic Press, an imprint of Elsevier, Amsterdam Boston Heidelberg, Third edition., 2013.
50 N. Davydov, A. Mustafina, V. Burilov, E. Zvereva, S. Katsyuba, L. Vagapova, A. Konovalov and I. Antipin, *ChemPhysChem*, 2012, **13**, 3357–3364.
51 M. Cheng, L. Zhou, J. Ma, J. Mu, C. Yi and M.-J. Li, *Mater. Sci. Eng. C*, 2019, **104**, 109972.
52 J. Pellico, C. M. Ellis and J. J. Davis, *Contrast Media Mol. Imaging*, 2019, **2019**, 1–13.
53 W. J. Rieter, J. S. Kim, K. M. L. Taylor, H. An, W. Lin, T. Tarrant and W. Lin, *Angew. Chem. Int. Ed.*, 2007, **46**, 3680–3682.
54 F. Carniato, L. Tei, W. Dastrù, L. Marchese and M. Botta, *Chem. Commun.*, 2009, 1246–1248.
55 J. Choi, J.-H. Lee, T.-H. Shin, H.-T. Song, E. Y. Kim and J. Cheon, *J. Am. Chem. Soc.*, 2010, **132**, 11015–11017.